NEUROSCIENCE

Thalamo-hippocampal pathway determines aggression and self-harm

Jane Jung[1,2], In-Jee You[1,2], Sora Shin[1,2,3]*

Aggression and self-harm are maladaptive coping strategies that often occur in individuals with a history of early life trauma (ELT), yet their underlying neural mechanisms remain unclear. Here, we identify L-type calcium channel (LTCC)–expressing thalamic nucleus reuniens (RE) as a critical component regulating both behaviors. ELT-induced excessive LTCC activity in vesicular glutamate transporter 2 (vGlut2) RE neurons and its corresponding effects on persistent neuronal activation contribute to increasing susceptibility to aggression and self-harm. Activation of vGlut2 RE neurons projecting to ventral hippocampus (vCA1), but not medial prefrontal cortex, promotes these behaviors in control mice. Furthermore, we found that RE neurons modulate two distinct subsets of vCA1 neurons, with one projecting to the hypothalamus to drive aggression and another to the basal amygdala to mediate self-harm. Our findings uncover how LTCC functions in the RE-to-vCA1 neural pathway increase the risk of aggression and self-harm, highlighting potential therapeutic targets for mitigating destructive behaviors following early adversity.

INTRODUCTION

Aggression encompasses actions intended to cause harm or damage to others, while self-harm refers to the deliberate infliction of physical injury on oneself. These behaviors are adopted as maladaptive coping strategies in response to emotional distress, particularly in individuals with a history of early life trauma (ELT) characterized by a disruption of early social bonding with primary caregivers (*1*–*3*). Notably, there is a positive correlation between aggression and self-harm, with individuals who have received clinical care for self-inflicted injuries being five times more likely to be convicted of excessive aggression and violence than those who with no history of self-harm (*4*–*7*). It remains unknown, however, whether aggression and self-harm arise from pathophysiology in a shared neural circuit and, if so, how the function of that circuit is affected by adverse experiences, such as ELT.

L-type calcium channels (LTCCs) belong to the calcium voltage-gated channel subunit alpha1 (*Cacna1*) gene family, with *Cacna1c* ($Ca_v1.2$) and *Cacna1d* ($Ca_v1.3$) being the main subtypes expressed in the brain (*8*). These channels have been associated with ELT and implicated in several psychiatric symptoms (*9*–*11*). For example, excessive LTCC activity impairs how social information is interpreted and elevates the risk of aggression (*12*–*14*). LTCCs are also implicated in self-harm; not only does pharmacological LTCC inhibition reduce self-harm rates in patients with psychiatric disorder (*15*, *16*), but systemic administration of the LTCC agonist (±) Bay K 8644 (Bay K) also induces self-biting and self-injury behaviors in mice (*17*). These lines of evidence indicate that LTCCs serve as key molecular targets capable of integrating and transmitting aggression- or self-harm–relevant signals, yet it is still unknown how the circuit-specific LTCC functions contribute to these maladaptive behaviors following ELT.

The nucleus reuniens (RE) of the midline thalamus serves as a critical hub within an extensive network that connects hippocampal and cortical structures. As an important convergent point, RE integrates diverse inputs from multiple cortical and subcortical regions, playing a key role in regulating cognitive and emotional functions as well as pain sensation (*18*–*20*). Recent studies have shown the necessity of reciprocal connectivity between the medial prefrontal cortex (mPFC) and RE for social information processing (*21*). In addition, selective increases in 5-hydroxytryptamine neurotransmitter system in the RE have been implicated in early life stress–induced nociceptive hypersensitivity (*20*). However, it is still unknown how the RE activity contributes to heightened vulnerability to aggression or self-harm following ELT and whether specific molecular changes within the RE circuitry are responsible for these effects.

In this study, we investigated the role of LTCC-expressing RE circuitry in driving aggression and self-harm potentially via modulation of pain sensitivity. We found that RE serves as the critical site where treatment with the LTCC agonist Bay K induces aggression and self-biting/self-injury behaviors in mice. Notably, LTCC activity in vesicular glutamate transporter 2 (vGlut2) RE neurons was significantly up-regulated in mice exposed to ELT, which exhibited heightened baseline aggression and increased susceptibility to Bay K–induced self-harm. RE-specific *Cacna1c* deletion in ELT mice mitigated these maladaptive behavioral features. Microendoscopic calcium imaging of in vivo neuronal activity revealed that ELT exposure rendered vGlut2 RE neurons persistently active in response to social stimuli or submaximal doses of Bay K administration, thereby contributing to enhanced aggression and self-harming behaviors. Activity of the ventral hippocampus (vCA1)–projecting vGlut2 RE (vGlut2 RE➔vCA1) neurons was necessary for the expression of these behaviors. This circuit activity was also required for the induction of exaggerated pain–like states, which potentially contributed to the emergence of heightened aggression and self-harm in ELT mice. We further identified that RE neurons mediate aggression and self-harm by modulating two distinct subsets of vCA1 neurons: one that projects to the hypothalamus (Hypoth) to promote aggression and another that projects to the basal amygdala (BA) to mediate self-harm associated with pain. Together, these discoveries provide a previously unknown framework for understanding the shared neural mechanisms underlying both aggression and self-harm, which

[1]Fralin Biomedical Research Institute at VTC, Roanoke, VA, USA. [2]FBRI Center for Neurobiology Research, Roanoke, VA, USA. [3]Department of Human Nutrition, Foods, and Exercise, Virginia Polytechnic Institute and State University, Blacksburg, VA, USA. *Corresponding author. Email: srshin@vtc.vt.edu

highlights LTCC-expressing RE neurons as an important component for integrating internal and external signals and functionally directing the vCA1 circuit to increase the risk of maladaptive responses, such as aggression and self-harm.

RESULTS

LTCC activation induces aggression and self-harm, both accompanied by pain

To investigate the effects of pharmacological activation of LTCCs on aggression and self-harm, we administered Bay K to adult mice (6 to 8 weeks old) in an escalating-dose paradigm. Low doses of Bay K [0.01 to 0.1 mg/kg, subcutaneously (sc)] induced excessive aggression in male but not female mice, as evidenced by a shorter latency to first attack, as well as increased attack duration and frequency during a 10-min resident-intruder (RI) assay (Fig. 1, A to D). These aggression-enhancing effects of low-dose Bay K (0.1 mg/kg, sc) occurred without affecting baseline locomotion but were accompanied by increased sensitivity to mechanical and thermal stimuli as measured by von Frey and hot plate tests (Fig. 1, E and F, and fig. S1, A to C).

To further determine whether the observed mechanical hypersensitivity represents pain state, we used high-speed videography

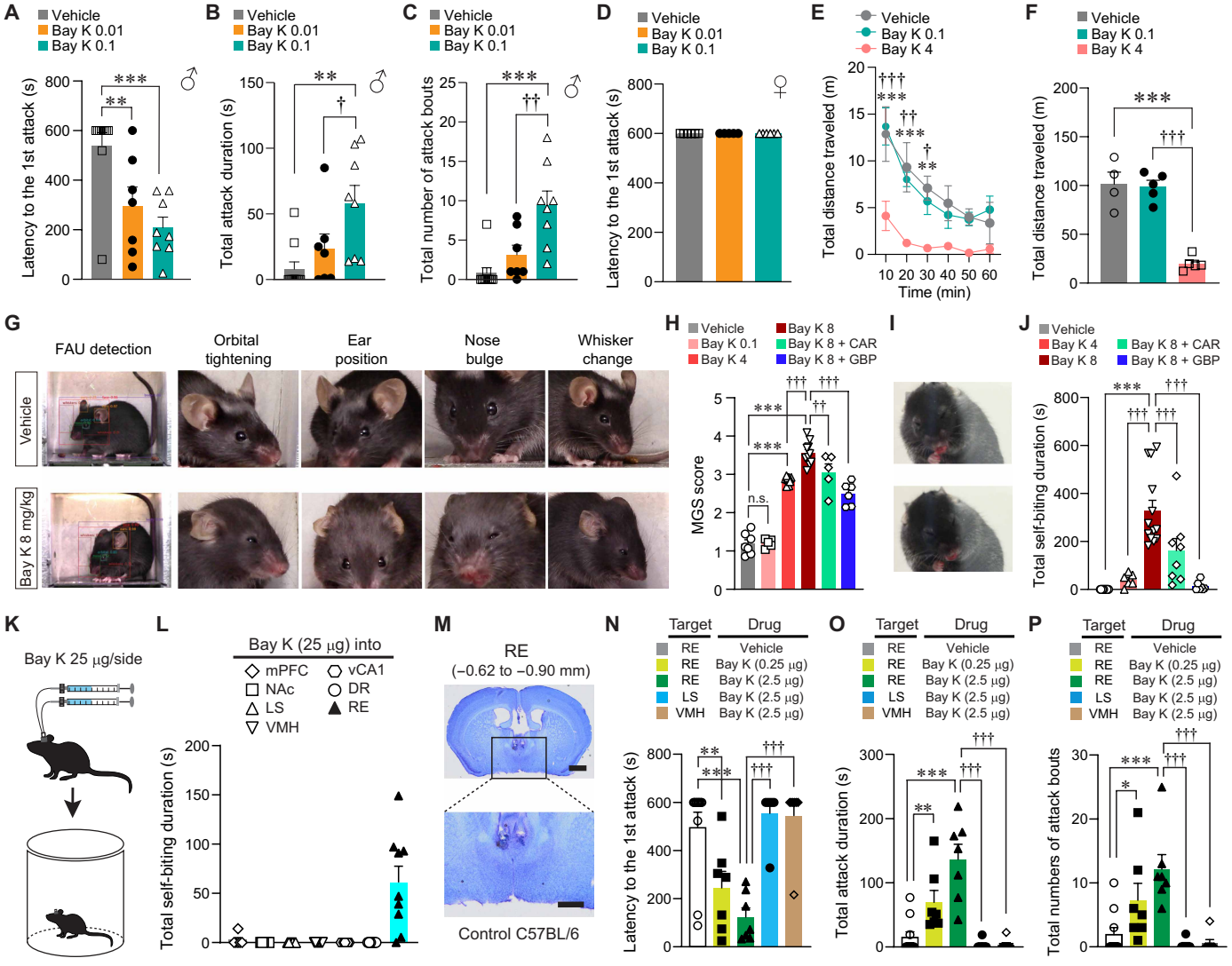

Fig. 1. LTCC activation in the RE induces aggression and self-harming behaviors. (**A** to **D**) Bay K administration (0.01 or 0.1 mg/kg, sc) increased aggressive behaviors in males [(A) to (C)] (n = 10, 7, and 8 mice), but not females (D) (n = 6, 5, and 6 mice), with a shortened attack latency, prolonged attack duration, and an increased number of attack bouts. (**E** and **F**) Bay K (4 mg/kg, sc) impaired locomotion (n = 4, 5, and 5 mice). (**G**) Example photographs of facial grimaces in mice treated with either vehicle or Bay K (8 mg/kg, sc). (**H**) MGS scores following Bay K injections with or without pretreatment of CAR or GBP (n = 7, 6, 10, 10, 5, and 6 mice). (**I**) Example photographs of self-biting behaviors in Bay K (8 mg/kg, sc)–injected mice. (**J**) Self-biting behavior following Bay K injections with or without pretreatment of CAR or GBP (n = 13, 6, 13, 8, and 7 mice). (**K**) Schematic for microinfusion of Bay K (25 μg per side) into the local brain regions. (**L**) Microinjection of Bay K into the RE increased self-biting behaviors (n = 6, 7, 7, 8, 7, 7, and 9 mice for mPFC, NAc, LS, VMH, vCA1, DR, and RE, respectively). (**M**) Location of cannula tips in the RE. Scale bars, 1 mm (top) and 500 μm (bottom). (**N** to **P**) Dose-dependent increase in aggression following Bay K microinjection into the RE (n = 10, 7, 7, 6, and 7 mice), demonstrated by a shortened attack latency, increased attack duration, and bout number. Statistical analyses with significance: one-way analysis of variance (ANOVA) [(A) to (C), (F), (H), (J)], and [(N) to (P)] and two-way repeated-measures (RM) ANOVA (E); *P < 0.05; **P < 0.01; ***P < 0.001; †P < 0.05; ††P < 0.01; †††P < 0.001. n.s., not significant. Data are presented as means ± SEM.

(2000 frames/s) to capture subsecond paw withdrawal movements in responses to mid-force von Frey filament (0.4 g) stimulation (*22*–*24*). Using Social LEAP Estimates Animal Poses (SLEAP) pose estimation and pain assessment at withdrawal speeds (PAWS) analysis (*25*), we extracted behavioral features indicative of pain, including affective coping responses such as paw shaking and paw guarding. Bay K treatment (0.1 mg/kg, sc) significantly increased paw guarding compared to vehicle-treated mice, while paw shaking remained unchanged (fig. S1, D and E). These results suggest that low-dose Bay K partly increases the affective motivational aspect of pain, rendering mice more sensitive to physical stimuli. Given that the heightened pain state can change the way individuals interact with the environment and negatively affect social information processing (*26*, *27*), low-dose Bay K (0.1 mg/kg, sc) likely contributes to the emergence of aggression, as a defensive reaction to prevent further discomfort.

At a dose of 4 mg/kg (sc), Bay K administration disrupted general movement (Fig. 1, E and F), while the highest dose we tested (8 mg/kg, sc) triggered significant motor abnormalities, including abnormal postures and reduced rearing (fig. S1, F and G). These mice also emitted human-audible distress calls (i.e., squeaks) (fig. S1H), indicating that they were in an aversive state, likely experiencing pain (*28*, *29*).

To validate the presence of pain in mice treated with high-dose Bay K (8 mg/kg, sc), we used the PainFace software platform to score facial grimaces, a reliable indicator of spontaneous pain (*30*, *31*). The mouse grimace scale (MGS) in C57BL/6 mice consists of four facial action units (FAUs): orbital tightening (closed eyes), ear position, nose bulge, and whisker change (*30*). We found that the mean MGS score of Bay K–treated mice increased significantly and remained elevated throughout the 30-min test session, with a dose-dependent manner (Fig. 1, G and H, and fig. S1I). To further determine whether this grimacing behavior reflected pain, we assessed the effects of two commonly used analgesics in veterinary or human medicine, such as carprofen (CAR) or gabapentin (GBP) (*32*–*34*), on Bay K–induced MGS scores. Pretreatment with either CAR or GBP delayed or prevented the increases of MGS scores following Bay K (8 mg/kg, sc), confirming the presence of ongoing pain in these mice (Fig. 1H and fig. S1I). In addition, we quantified the percentage of video frames falling into low (0 to 2), medium (3 to 4), and high (5 to 8) MGS score categories. While most of frames from the vehicle group (90.6%) fell into the low grimace category, 44.1 and 25.8% of frames from Bay K (8 mg/kg, sc)–injected mice fell into the medium and high grimace categories, respectively. Notably, GBP pretreatment markedly reduced these proportions to 31.3% (medium) and 12.2% (high), confirming that Bay K–induced MGS reflects pain-based responses (fig. S1J).

These grimacing mice also exhibited self-biting behavior, characterized by gnawing on parts of their own bodies (e.g., fore/hind paws) (Fig. 1, I and J, and fig. S1K). Unlike surface-level licking observed during self-grooming, this self-biting behavior resulted in visible skin injuries within the 40-min test session (fig. S1, L to O). Even when provided with alternative chewable objects such as wood blocks or nylon items, mice consistently directed their biting toward themselves (fig. S1, P and Q). Similarly, these mice continued to engage in self-biting behaviors in the presence of appetitive stimuli, including a social target or high-fat diet, showing little to no interest in interacting with or consuming them (fig. S1, R to T), suggesting that Bay K–induced biting behavior is selectively self-directed. Notably, pretreatment with either CAR or GBP, which alleviates spontaneous pain (Fig. 1H), significantly suppressed the self-biting behavior (Fig. 1J). This supports the idea that Bay K–treated mice may engage in self-harm in a maladaptive attempt to counteract their experience of pain. Together, these results demonstrate two distinct behavioral outcomes following Bay K administration: Low doses (0.01 to 0.1 mg/kg, sc) primarily enhance aggression, while high doses (4 to 8 mg/kg, sc) elicit self-harming behaviors—both behaviors are accompanied by indicators of pain.

Activation of LTCCs in the RE induces aggression and self-harm

Both aggression and self-harm are likely triggered via the integration of sensory and affective aspects of pain that are associated with negative emotional states, such as fear, anxiety, or impulsivity (*35*–*38*). Among the brain regions implicated in this process, the RE is a crucial node that integrates cognitive and affective information and regulates associated behaviors via extensive connection to hippocampal and cortical structures (*21*, *39*–*41*). Moreover, among the various brain regions that express LTCCs, the RE expresses relatively higher amounts of $Ca_v1.2$ and $Ca_v1.3$ than other aggression-related regions such as the lateral septum (LS) (*42*, *43*) and ventromedial hypothalamus (VMH) (*44*, *45*) (fig. S2A).

We first asked whether LTCC activation in the RE could directly induce self-harm. Local infusion of Bay K into the RE (25 μg per side) robustly induced self-biting behaviors in mice, comparable to those triggered by a systemic Bay K administration. In contrast, similar local infusions into other regions, including the mPFC, nucleus accumbens (NAc), LS, VMH, vCA1, and dorsal raphe (DR), did not induce these behaviors (Fig. 1, K to M, and fig. S2, B to H). This suggests that the RE is a key site for mediating Bay K–induced self-harming behaviors.

Given that aggression occurred at lower doses of systemic Bay K than those required to induce self-harm (Fig. 1, A to C), we next investigated whether an intracranial infusion of low-dose Bay K (0.25 or 2.5 μg per side) into the RE could promote aggression. We found that Bay K–infused mice exhibited a dose-dependent increase in aggressive behaviors during RI tests, as indicated by a reduced latency to first attack and increased attack duration/frequency. Notably, this enhanced aggression was not observed when the same doses of Bay K were infused into previously identified aggression-related brain regions, such as the LS or VMH (Fig. 1, N to P), indicating that the RE is specialized for mediating LTCC activation–induced aggression.

Increased aggression is often associated with anxiety, which can make individuals more sensitive to potential social threats (*46*, *47*). We therefore asked whether the aggressive phenotype we observed in Bay K–treated mice was accompanied by increased anxiety in a novel environment. At the aggression-enhancing dose (2.5 μg per side), Bay K–infused mice displayed enhanced anxiety–like behavior, spending significantly more time in the periphery zone and less time in the center zone of an open-field arena, without any associated changes in locomotor activity (fig. S3, A to E). This suggests that LTCC activation in the RE disrupts emotional regulation and increases anxiety, which may, in turn, provoke aggressive outbursts in social contexts. Collectively, these data support the hypothesis that RE is a critical neural substrate in which LTCC activation increases susceptibility to both aggression and self-harm.

ELT increases susceptibility to aggression and self-harm

LTCCs are known to be involved in physiological and molecular adaptations to ELT, a significant risk factor for the development of

various psychiatric disorders (*9*, *10*). To investigate the impact of ELT on aggression and self-harm, we used an ELT paradigm in which mouse pups were individually isolated from their dam and littermates for 23 hours at postnatal day 3 (P3) (*48*). Consistent with previous studies highlighting the hallmarks of early life stress (*49*, *50*), adult mice exposed to ELT exhibited heightened sensitivity in corticosterone levels—the end-product of the hypothalamic-pituitary-adrenal axis—following acute restraint stress (fig. S4, A and B). In addition, these mice displayed increased anxiety–like behaviors on the next day, spending more time in safe zones, such as the closed arms of the elevated plus maze and the peripheral area of the open field test (OFT) (fig. S4, C to E). Together, these findings confirm that ELT induces long-term physiological changes, including heightened hormonal and behavioral stress responses that last into adulthood.

We next sought to determine how ELT affects aggression and self-harm. In the RI test, ELT male mice exhibited escalated aggression, initiating their first attack more rapidly and engaging in prolonged attacks with a greater number of bouts compared to controls (Fig. 2, A to E). To determine whether ELT also exacerbates self-harming behaviors, we administered a submaximal dose of Bay K (4 mg/kg, sc), which typically induces only minor self-biting in control mice (Fig. 1J). ELT mice, however, exhibited intense self-biting/self-injury behaviors, resulting in severe wounds on accessible body parts, including the fore/hind paws, chest, and shoulders (Fig. 2, F to J). These findings indicate that ELT enhances susceptibility to maladaptive behavioral responses, amplifying both aggression and self-harm.

To determine whether the RE is preferentially involved in the exacerbated self-harming behaviors in ELT mice, we quantified the expression of c-fos, a neural activity marker, following administration of a submaximal dose of Bay K (4 mg/kg, sc). In control mice, Bay K–induced c-fos expression was observed in the RE, while we found a much larger induction of c-fos in the RE of ELT mice under the same conditions (Fig. 2, K and L). These results support the idea that ELT sensitizes RE neuronal responsiveness to Bay K, thereby increasing susceptibility to self-harm at a submaximal dose.

This led us to hypothesize that ELT increases endogenous LTCC activity in the RE, driving enhanced neuronal responses and associated behavioral consequences. Quantitative real-time polymerase chain reaction (qPCR) results revealed a significant increase in *Cacna1c* and *Cacna1d* mRNA levels in the RE of ELT mice compared to controls, whereas the expression of the calcium-binding proteins *Calb1* and *Calb2* remained unchanged regardless of ELT history (fig. S5A). Elevated *Cacna1c* mRNA expression was also detected in the mPFC, albeit to a lesser extent than for the RE, while no substantial changes were observed in other brain areas, such as the NAc, LS, VMH, vCA1, or DR (fig. S5B). Given that LTCC-expressing RE neurons are glutamatergic (fig. S5, C and D), we sought to further confirm whether the vGlut2 RE neurons of ELT mice show a similar up-regulation of LTCCs for genes actively being translated into proteins. To test this, we used viral translating ribosome affinity purification (vTRAP) (*51*). After injecting AAV-Flip-Excision (FLEX)-EGFP fused to ribosomal protein L10a (EGFPL10a) into the RE of vGlut2-Cre mice, we performed an anti–enhanced green fluorescent protein (EGFP) immunoprecipitation to purify translating mRNA from EGFPL10a-expressing vGlut2 RE neurons (Fig. 2M). Upon qPCR analysis of the resulting vTRAP RNA, we found significant increases in both *Cacna1c* and *Cacna1d* expression following ELT, but no changes were observed for *Calb1*, *Calb2*, N-terminal EF-hand calcium binding protein 1 (*Necab1*), or troponin T1, slow skeletal (*Tnnt1*) expression (Fig. 2N). This result suggests that the selective up-regulation of LTCCs in vGlut2 RE neurons is a critical molecular signature of ELT mice.

We next reasoned that ELT-induced up-regulation of LTCC activity in the RE is necessary for driving both aggression and self-harm. To test this, we administered a local infusion of the LTCC antagonist nicardipine (1 or 5 μg per side) into the RE—a treatment that had no effect on general locomotor activity (fig. S5, E and F)—and then subjected the mice to either an RI test or a submaximal dose of Bay K. Unlike vehicle-treated ELT mice, nicardipine-treated ELT mice exhibited reduced aggression, characterized by delayed first attack initiation and reduced total attack duration/frequency (fig. S5, G to I). Furthermore, the same drug treatment mitigated the exacerbated self-biting behavior observed in ELT mice following a submaximal dose of Bay K (fig. S5, J and K). Collectively, these data suggest that enhanced LTCC activity in the RE is required for mediating the heightened aggression and self-harm associated with ELT.

Of the two subtypes of LTCCs expressed in the brain, the excessive activity of *Cacna1c* ($Ca_v1.2$) has been implicated in the hormonal and behavioral stress responses associated with the increased risk of psychiatric disorders (*9*, *52*). We therefore reasoned that selective down-regulation of *Cacna1c* in the RE may rescue heightened aggression and self-harm observed in ELT mice. Using $Cacna1c^{flox/flox}$ mice, we confirmed that injection of AAV5-Cre into the RE of controls results in an 80% reduction of *Cacna1c* expression without affecting *Cacna1d* expression (Fig. 2O). Fluorescent in situ hybridization (FISH) results further revealed that the deletion of *Cacna1c* predominantly occurred in vGlut2 RE neurons (Fig. 2P). During RI tests, we found that RE-specific *Cacna1c* deletion normalized the hyperaggressive behaviors of ELT mice, delaying first attack onset and reducing total attack duration/frequency (Fig. 2, Q to S). Furthermore, these ELT mice with RE-specific *Cacna1c* deletion showed reduced self-biting behaviors following a submaximal dose of Bay K injection (Fig. 2T). These data demonstrate that $Ca_v1.2$ in the RE is necessary for the increased susceptibility to aggression and self-harm following ELT.

vGlut2 RE neurons are hyperactive in ELT mice during aggression and self-harm

Given the critical role of LTCCs in regulating neuronal activity (*53*, *54*), we hypothesized that ELT mice may exhibit dysregulated vGlut2 RE neuronal activity in social contexts. To test this, we performed real-time imaging of the genetically encoded calcium indicator GCaMP6f through an intracranial gradient index (GRIN) lens, acquiring single cell–resolution in vivo Ca^{2+} imaging data before and after exposure to nonsocial (i.e., a fake mouse) or social (i.e., a conspecific stranger) stimuli (Fig. 3, A to C). In control mice, in vivo vGlut2 RE neuronal activity peaked at the first social contact with a stranger mouse (i.e., nose-to-nose interaction). This was followed by a rapid suppression of GCaMP6 fluorescence that remained below baseline during normal social activities (i.e., sniffing, following, and mounting) (Fig. 3E and fig. S6, A and B). However, we did not observe any significant changes in vGlut2 RE activity in response to interactions with a fake mouse (Fig. 3D). These findings suggest that the initial vGlut2 RE neuronal activity peak is specifically engaged in the first stage of social information processing, while subsequent suppression of vGlut2 RE neurons may help prevent excessive engagement with social stimuli, allowing mice to maintain naturalistic social interactions.

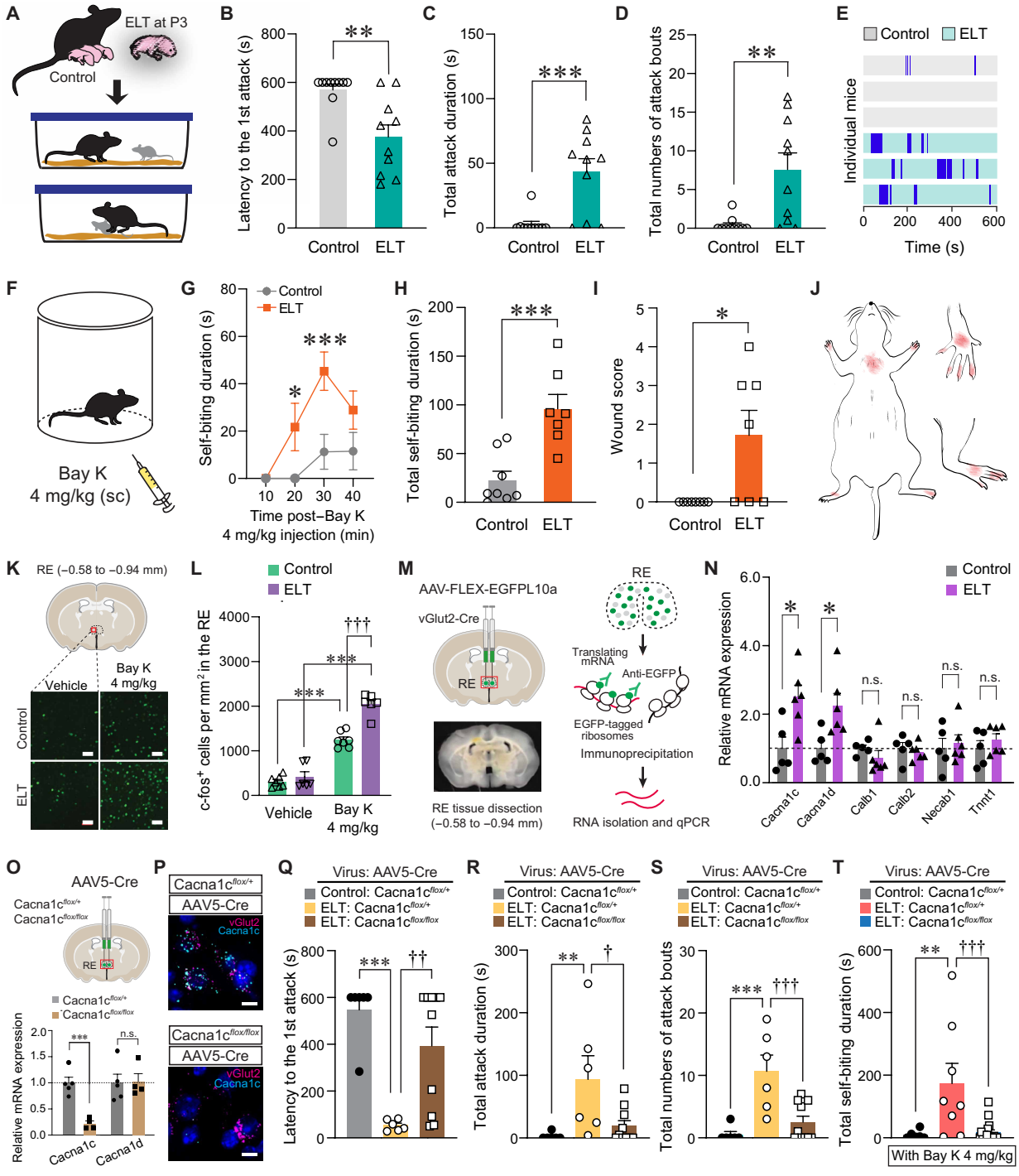

Fig. 2. Elevated aggression and self-harm in ELT mice with excessive LTCC activity in the RE. (**A**) Schematic of the ELT procedure and RI test. (**B** to **D**) ELT male mice exhibited increased aggression ($n = 10$ and 10 mice), with a shortened attack latency and enhanced attack duration and number. (**E**) Raster plots of attack bouts from three control or ELT mice. (**F**) Schematic of setup for monitoring Bay K (4 mg/kg, sc)–induced self-biting behavior. (**G** to **I**) ELT mice showed exacerbated self-biting and more severe wounds ($n = 8$ and 7 mice). (**J**) Diagram summarizing locations of wounds induced by self-biting behaviors (highlighted in red). (**K**) Images of the RE showing c-fos staining. Scale bars, 50 μm. (**L**) Quantification of c-fos–positive cells in the RE ($n = 7$, 6, 7, and 6 mice). (**M**) Schematic of AAV-FLEX-EGFPL10a injection into the RE of vGlut2-Cre mice and vTRAP method. (**N**) qPCR analysis of immunoprecipitated mRNAs from (M) ($n = 5$ and 6 replicates). (**O**) Schematics of AAV5-Cre injection into the RE of *Cacna1c*$^{flox/+}$ or *Cacna1c*$^{flox/flox}$ mice. qPCR analysis of *Cacna1c* and *Cacna1d* mRNA expression ($n = 5$ and 4 mice). (**P**) Images of FISH for vGlut2 and *Cacna1c* in the RE, replicated independently in three mice. Scale bars, 10 μm. (**Q** to **S**) Cre-induced *Cacna1c* deletion in the RE-reduced aggression in ELT mice ($n = 6$, 6, and 10 mice), with enhanced attack latency and reduced duration and number. (**T**) Self-biting behaviors after a submaximal Bay K injection ($n = 6$, 8, and 17 mice). Statistical analyses with significance: two-tailed unpaired *t* test [(B) to (D), (H), (I), (N), and (O)], two-way RM ANOVA (G), two-way ANOVA (L), one-way ANOVA [(Q) to (T)]; *$P < 0.05$; **$P < 0.01$; ***$P < 0.001$; †$P < 0.05$; ††$P < 0.01$; †††$P < 0.001$. Data are presented as means ± SEM.

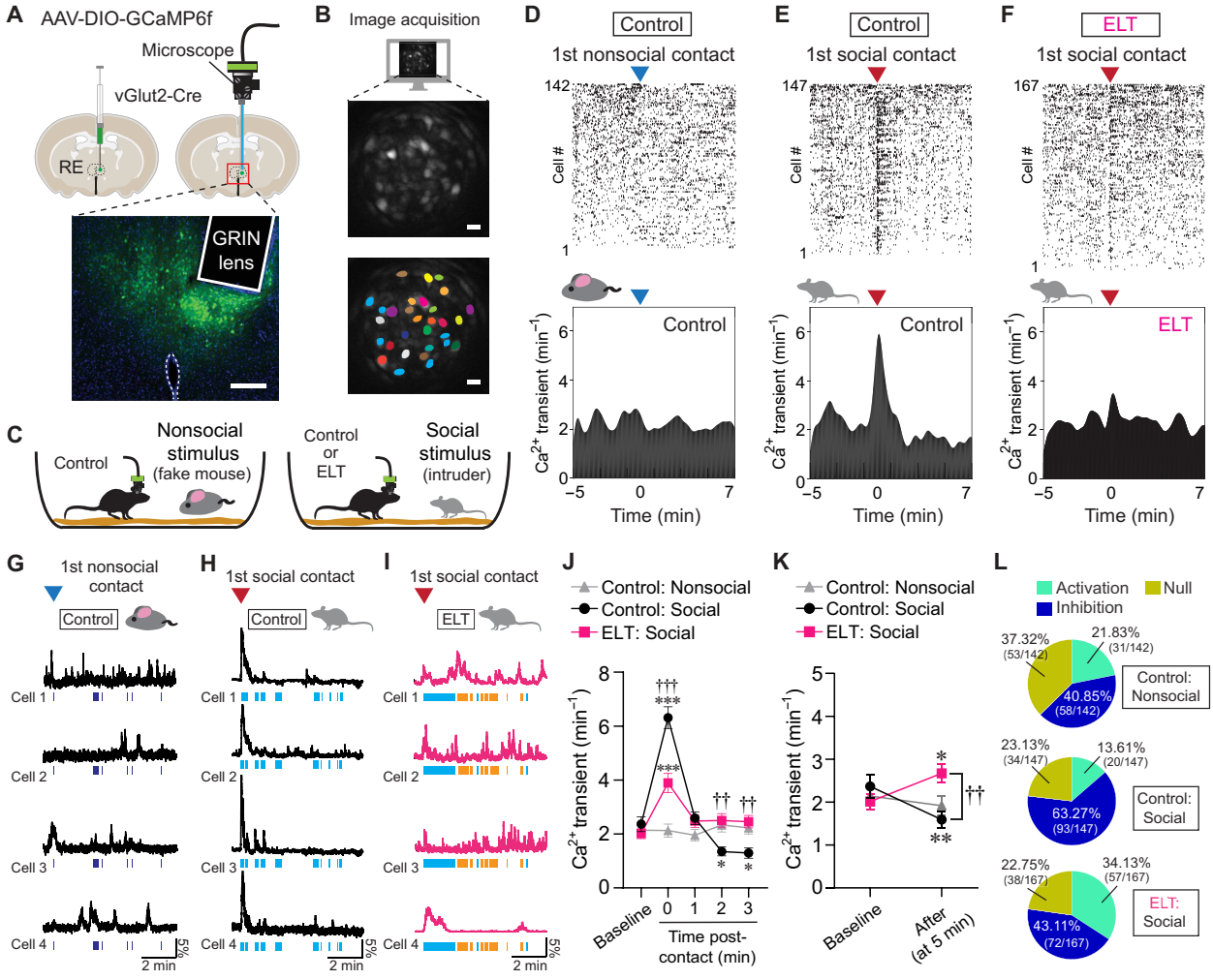

Fig. 3. Dysregulated vGlut2 RE neuronal activity of ELT mice in response to social stimulus. (**A**) Schematic and image of AAV-DIO-GCaMP6f expression and GRIN lens implantation in the RE. Scale bar, 200 μm. (**B**) Sample image of GCaMP6f-expressing vGlut2 RE neurons and the color-coded regions of interest. Scale bars, 200 μm. (**C**) Schematic illustrating the experimental setup for recording vGlut2 RE in vivo neuronal activity in response to a fake mouse (nonsocial) or an unfamiliar intruder (social). (**D** and **E**) Raster plots (top) and peristimulus time histograms (bottom) showing vGlut2 RE neuronal activity of control mice upon first contact with a fake mouse (D) or an intruder (E). In the raster plots, each row represents an individual cell, and each tick denotes a single Ca^{2+} transient event. Blue and red arrowheads mark the time of first contact with a fake mouse and the intruder mouse, respectively. (**F**) Same as (E), but for ELT mice. (**G** to **I**) Representative Ca^{2+} activity traces from vGlut2 RE neurons following first contact with a fake mouse or an intruder. Dark- and light-blue–shaded areas indicate physical interaction bouts with a fake mouse or an intruder, while orange-shaded areas indicate attack bouts. (**J**) Time course of Ca^{2+} transients per minute, measured during baseline and after first contact with a fake mouse ($n = 142$ cells) or intruder ($n = 147$ and 167 cells). (**K**) Differential vGlut2 RE neuronal responses 5 min after the first contact, from the cells shown in (J). (**L**) Pie charts categorizing vGlut2 RE neuronal responses (activation, null, and inhibition) after first contact with either a nonsocial or social stimulus. Statistical analyses with significance: two-way RM ANOVA [(J) and (K)]; $*P < 0.05$; $**P < 0.01$; $***P < 0.001$; $††P < 0.01$; $†††P < 0.001$. Data are presented as means ± SEM.

In contrast to this fine regulation, vGlut2 RE neurons of ELT mice exhibited a blunted response to initial social contact and sustained activation during subsequent social activities, including attack bouts (Fig. 3, F to K, and fig. S6, C to E). Notably, a larger proportion of vGlut2 RE neurons in ELT mice (34.13%) remained active after the first social contact, compared to control mice exposed to either social (13.61%) or nonsocial (21.83%) stimuli (Fig. 3L). These findings substantiate the idea that a typical "sharp peak–and–suppression" pattern of social stimulus–induced vGlut2 RE activity is disrupted in ELT mice. Instead, we found that ELT mice exhibited a blunt peak–and–no suppression activity pattern characterized by persistent vGlut2 RE neuronal activation during altered social reactions, such as aggression.

We next asked how well in vivo vGlut2 RE neuronal activity correlates with the occurrence of self-biting behaviors after Bay K administration. Since LTCC activation stimulates Ca^{2+} influx (*55*), we first assessed how the different doses of Bay K influence baseline in vivo Ca^{2+} dynamics of vGlut2 RE neurons. We observed a dose-dependent increase in the average number of Ca^{2+} transients per minute in the vGlut2 RE neurons after systemic Bay K treatments (Fig. 4, A and B), confirming that Bay K–induced LTCC activation effectively enhances vGlut2 RE neuronal activity.

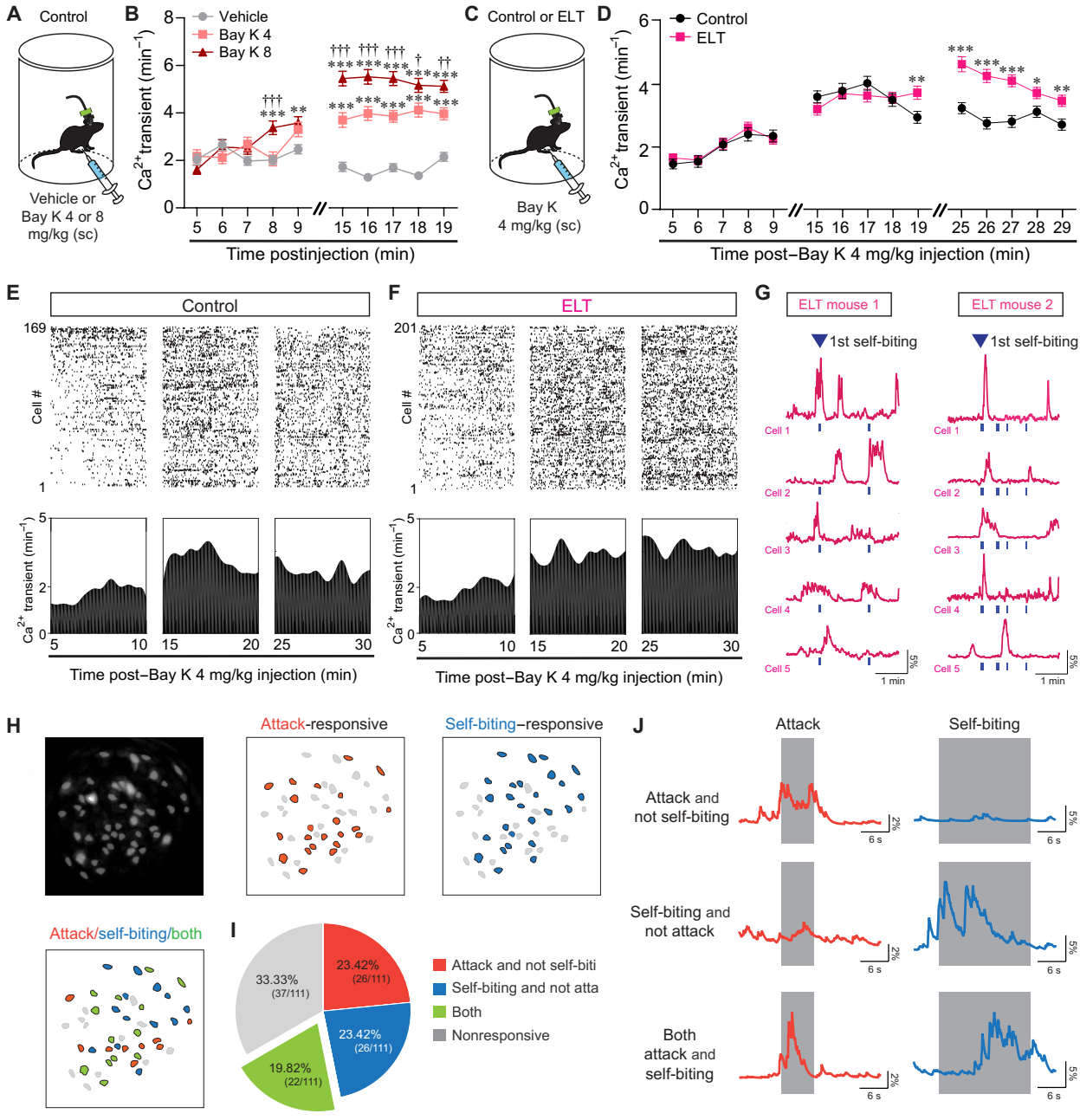

Fig. 4. Persistent vGlut2 RE neuronal activation of ELT mice after Bay K administration. (**A**) Schematic illustrating the recording of vGlut2 RE in vivo neuronal activity after Bay K treatments. (**B**) Time course of Ca^{2+} transients per minute, measured after vehicle or Bay K administration ($n = 122$, 116, and 126 cells). (**C**) Schematic illustrating in vivo Ca^{2+} imaging of mice treated with Bay K (4 mg/kg, sc). (**D**) Time course of Ca^{2+} transients per minute, measured at 5, 15, and 25 min postinjection ($n = 169$ and 201 cells). (**E** and **F**) Raster plots and peristimulus time histograms showing vGlut2 RE neuronal activity of control (E) and ELT (F) vGlut2-Cre mice after administration of submaximal Bay K. The rows and ticks in the raster plots represent individual cells and single Ca^{2+} transient events, respectively. (**G**) Examples of individual traces of vGlut2 RE neuronal activity from two ELT mice during self-biting after Bay K injections (4 mg/kg, sc). Dark blue shaded areas indicate self-biting bouts. (**H**) Example field of view showing vGlut2 RE neurons from ELT mice, color-coded by response type: attack-responsive (orange), self-biting-responsive (blue), and both behaviors (light green). (**I**) Pie charts summarizing the proportions of ELT vGlut2 RE neurons ($n = 111$ cells) that responded to attack only, self-biting only, both behaviors, or neither. (**J**) Representative traces of individual vGlut2 RE neurons from ELT mice following attack or self-biting bouts: a neuron responsive to attack but not self-biting (top); one responsive to self-biting but not attack (middle); one responsive to both behaviors (bottom). Statistical analyses with significance: two-way RM ANOVA [(B) and (D)]; $*P < 0.05$; $**P < 0.01$; $***P < 0.001$; $\dagger P < 0.05$; $\dagger\dagger P < 0.01$; $\dagger\dagger\dagger P < 0.001$. Data are presented as means ± SEM.

Given that ELT mice showed more self-biting behaviors than controls in response to a submaximal dose of Bay K (Fig. 2, F to J), we next examined how ELT alters in vivo vGlut2 RE neuronal activity under this condition (Fig. 4C). ELT vGlut2 RE neurons showed more Ca^{2+} transients per minute with sustained responsiveness compared to controls (Fig. 4, D to F). This change was particularly pronounced at 25 to 30 min post–Bay K injection, which is aligned with the timing of the increase in self-biting behaviors of ELT mice (Fig. 2G). In addition, 46.93% of vGlut2 RE neurons in ELT mice produced Ca^{2+} transients at the onset of self-biting bouts (Fig. 4G and fig. S6F), suggesting that these neurons are primarily recruited during Bay K–induced self-harm.

We next compared how vGlut2 RE neurons of ELT mice responded to aggression versus self-harm. Within the same field of view, we monitored in vivo activity of vGlut2 RE neurons during episodes of attack and self-biting bout (Fig. 4H). Among all imaged neurons, 23.42% (26 of 111) responded to attack but not to self-biting, an equal proportion (26 of 111) responded to self-biting but not to attack. Notably, 19.82% (22 of 111) of neurons responded to both behaviors (Fig. 4, I and J), representing a functionally relevant subpopulation of vGlut2 RE neurons that preferentially encodes both aggression and self-harm. Together, these data suggest that sustained activation of vGlut2 RE neurons may serve as a shared hallmark of the heightened susceptibility to both behaviors observed in ELT mice.

This led us to hypothesize that artificially driving vGlut2 RE activation could recapitulate the maladaptive behaviors of ELT mice. To test this, we injected the RE of control vGlut2-Cre animals with AAV–double-floxed inverted open reding frame (DIO)–channelrhodopsin-2 (ChR2)–enhanced yellow fluorescent protein (eYFP) or AAV-DIO-eYFP and implanted optic cannulae over the viral injection site, allowing precise excitation of vGlut2 RE cells during RI tests or after Bay K administration (fig. S7, A and B). We found that optogenetic activation of vGlut2 RE neurons escalated aggression, reducing latency to first attack and increasing both attack duration and frequency, in a light intensity–dependent manner (fig. S7, C to E). Furthermore, ChR2-mediated stimulation of vGlut2 RE neurons exacerbated self-biting behavior in response to a submaximal dose of Bay K (fig. S7F). These data suggest that the activation of vGlut2 RE cell bodies in mice without previous exposure to ELT is sufficient to induce aggression and self-harm at levels comparable to those observed in ELT mice.

vGlut2 RE➔vCA1 projections bidirectionally control aggression and self-harm

The RE is highly interconnected with hippocampal and cortical structures, sending excitatory inputs to both structures (*56*). To examine the anatomical distribution of RE neurons projecting to the mPFC or vCA1, we injected cholera toxin subunit B (CTB) conjugated to Alexa Fluor 488 or Alexa Fluor 647 into the mPFC and vCA1, respectively (fig. S8A). Quantification of CTB-positive RE neurons revealed distinct patterns that vCA1-projecting neurons were located predominantly in the rostral and medial RE, while mPFC-projecting neurons were primarily situated in the caudal and lateral RE (fig. S8, B and C). We also identified only a small subset of RE neurons (<5%) that projected to both the mPFC and vCA1 (fig. S8C), consistent with prior studies (*57*–*59*).

To identify the synaptic targets of vGlut2 RE neurons, we labeled their presynaptic terminals by injecting AAV expressing spaghetti monster fluorescent protein (smFP)–synaptophysin in a Cre-dependent manner into the RE of vGlut2-Cre mice (fig. S8D). We then observed dense innervations in the mPFC, vCA1, and other regions, including the NAc, zona incerta (ZI), and BA (fig. S8E). Furthermore, to test whether vGlut2 RE neurons send collateralized axons to multiple targets, we examined vGlut2 RE neurons projecting to vCA1 (vGlut2 RE➔vCA1) by injecting vGlut2-Cre mice with a retrograde AAV expressing Cre-dependent Flippase (Flp) into vCA1 and an AAV expressing Flp-dependent EGFP into the RE (Fig. 5, A and B). We found that the vGlut2 RE➔vCA1 neurons predominantly project to the vCA1, with only a little portion of collateralized axons targeting other areas, such as the mPFC, ZI, and BA (Fig. 5, C and D).

Since vGlut2 RE➔mPFC and vGlut2 RE➔vCA1 neurons seem to be distinct subpopulations with minimal overlap, we hypothesized that each subpopulation provides a distinct contribution to aggression and self-harming behaviors. Given that the persistent activation of vGlut2 RE neurons is a hallmark of ELT mice (Figs. 3 and 4), we reasoned that selective activation of either vGlut2 RE➔mPFC or vGlut2 RE➔vCA1 neurons may recapitulate the behaviors of ELT mice. To test this, we bilaterally expressed Cre-dependent G_q-coupled designer receptors exclusively activated by designer drugs (DREADD), human M3 muscarinic designer receptor (hM3D), in the RE of control vGlut2-Cre mice. We then performed bilateral clozapine *N*-oxide (CNO) infusion through cannulae positioned above each target structure to chemogenetically activate vGlut2 RE neuronal terminals in each location (i.e., the mPFC or vCA1) (Fig. 5E). Upon encountering a conspecific stranger, CNO-mediated activation of vGlut2 RE➔vCA1 neurons significantly increased aggression, as evidenced by a shorter latency to first attack, longer attack duration, and increased attack bouts, whereas a similar activation of vGlut2 RE➔mPFC neurons did not induce these behaviors (Fig. 5, F to H). Furthermore, CNO-mediated activation of vGlut2 RE➔vCA1, but not vGlut2 RE➔mPFC neurons, potentiated self-biting behaviors following a submaximal dose of Bay K (Fig. 5I), suggesting that vGlut2 RE➔vCA1 neurons are more important in promoting both aggression and self-harm than vGlut2 RE➔mPFC neurons.

To further confirm the role of vGlut2 RE➔vCA1 neurons in driving aggression and self-harm, we used optogenetics by injecting AAV-DIO-ChR2-eYFP or AAV-DIO-eYFP into the RE and implanting optic cannulae over vCA1 in control vGlut2-Cre mice (fig. S9A). Consistent with our chemogenetic data (Fig. 5, F to H), optogenetic activation of vGlut2 RE neuronal terminals in vCA1 increased aggressive behaviors, reducing latency to first attack and increasing both attack duration/frequency in a light intensity–dependent manner (fig. S9, B to D). Furthermore, we found that blue light stimulation (20 Hz) of ChR2-expressing vGlut2 RE terminals in the vCA1 amplified self-biting behaviors following a Bay K injection (4 mg/kg, sc) (fig. S9, E and F). Together, these data indicate that chemogenetic and optogenetic activation of vGlut2 RE➔vCA1 neurons is sufficient to increase susceptibility to aggression and self-harm, mirroring the behavioral phenotypes observed in ELT mice.

vCA1 is a principal node in the neural circuitry implicated in regulating negative emotional states, such as anxiety (*60*, *61*). Because aggression and self-harm can be precipitated by negative emotional states, we next asked whether vGlut2 RE➔vCA1 neurons also transmit a negative valence signal. In a real-time place test (RTPT), we found that ChR2-mediated activation of vGlut2 RE➔vCA1 neurons caused mice to avoid the side of the RTPT apparatus paired

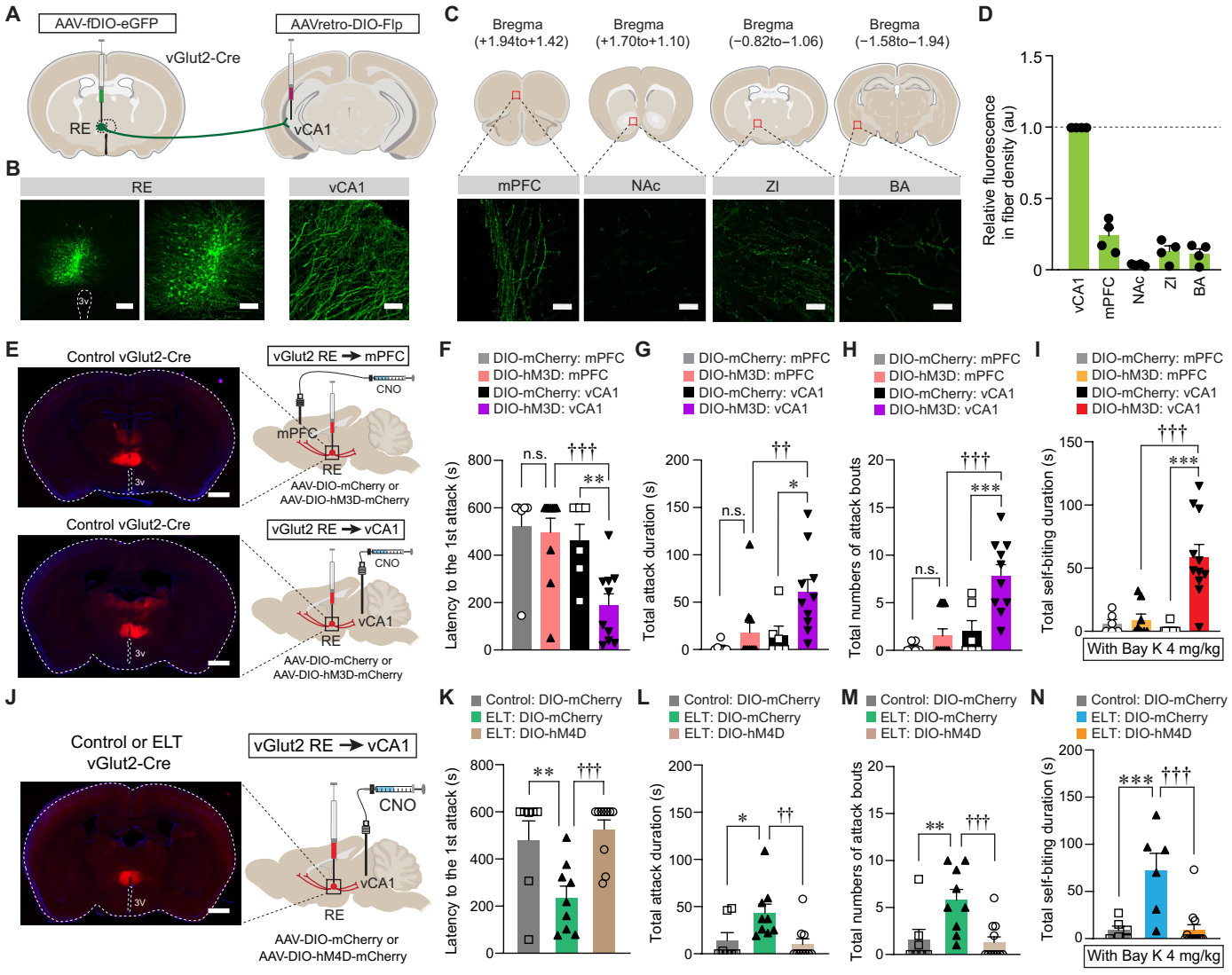

Fig. 5. vGlut2 RE➔vCA1 neurons mediate aggression and self-harm. (**A**) Schematic depicting injections of AAV-fDIO-EGFP and AAVretro-DIO-Flp into the RE and vCA1 of vGlut2-Cre mice, respectively. (**B**) Images of EGFP-labeled cell bodies in the RE and fibers in the vCA1. Scale bars, 200 μm (left), 100 μm (middle), and 50 μm (right). (**C**) Coronal views of the areas in which confocal images were taken (red squares). Images of fibers in target areas, including the mPFC, NAc, ZI, and BA. Scale bars, 50 μm. (**D**) Fiber density quantification from vGlut2 RE➔vCA1 neurons ($n = 4$ mice). au, arbitrary units. (**E**) Images showing vGlut2 RE neurons expressing hM3D-mCherry. Scale bars, 1 mm. Schematic for chemogenetic activation of vGlut2 RE➔mPFC or vGlut2 RE➔vCA1 neurons in vGlut2-Cre mice. (**F** to **H**) CNO-induced activation of vGlut2 RE➔vCA1 neurons, but not vGlut2 RE➔mPFC, increased aggressive behaviors ($n = 6$, 10, 6, and 10 mice) with a shortened attack latency and increased attack duration and attack number. (**I**) Bay K (4 mg/kg, sc)–induced self-biting behavior after CNO microinjection ($n = 6$, 8, 9, and 11 mice). (**J**) Images showing vGlut2 RE neurons expressing hM4D-mCherry. Scale bar, 1 mm. Schematic for chemogenetic inhibition of vGlut2 RE➔vCA1 neurons in ELT vGlut2-Cre mice. (**K** to **M**) CNO-induced inhibition of vGlut2 RE➔vCA1 neurons mitigated escalated aggression in ELT mice ($n = 7$, 9, and 10 mice), including delayed attack latency and decreased attack duration and attack number. (**N**) Bay K (4 mg/kg, sc)–induced self-biting behavior after CNO microinjection ($n = 6$, 6, and 13 mice). Statistical analyses with significance: one-way ANOVA [(F) to (I)] and [(K) to (N)]; $*P < 0.05$; $**P < 0.01$; $***P < 0.001$; $††P < 0.01$; $†††P < 0.001$. Data are presented as means ± SEM.

with photostimulation without affecting overall locomotor activity (fig. S9, G and H). Moreover, upon activation of the same circuit, these mice exhibited increased anxiety–like behaviors in an open-field arena, as indicated by reduced time spent in the center zone and a stronger preference for the periphery (fig. S9, I and J). Together, these data suggest that vGlut2 RE➔vCA1 neurons inherently encode negative valence signals, increasing the susceptibility to aggression in social contexts or self-harm following Bay K administration.

To determine whether inhibition of vGlut2 RE➔vCA1 neurons could reverse the aberrant behavioral phenotypes of ELT mice, we optogenetically or chemogenetically suppressed vGlut2 RE neuronal terminals using bilateral optic fibers or drug infusion cannulae positioned above the vCA1 (Fig. 5J and fig. S10A). When ELT mice encountered a social stimulus, optogenetic inhibition of vGlut2 RE➔vCA1 neurons reduced attack latency, duration, and frequency without any concurrent differences in locomotion (fig. S10, B to E). Similarly, CNO-mediated inhibition of vGlut2 RE➔vCA1 neurons

attenuated the aggression and self-harming behaviors of ELT mice (Fig. 5, K to N). These data suggest that optogenetic or chemogenetic silencing can mitigate the hyperactivity of vGlut2 RE➔vCA1 neurons in ELT mice, thereby normalizing their maladaptive behaviors, such as increased aggression and self-harm.

vGlut2 RE➔vCA1 circuit is necessary for increasing pain sensation in ELT mice

Because aggression and self-harm following Bay K administration are associated with pain that is often comorbid with negative emotional states (figs. S1 and S9), we hypothesized that ELT mice exhibit heightened pain sensation, which may contribute to their maladaptive behavioral phenotypes. Using a range of standard mechanical stimuli, we found that ELT robustly increased the behavioral responses to mid-force von Frey filaments (0.4 to 1.4 g) compared with controls (Fig. 6, A and B). To further determine whether these responses of ELT mice are accompanied by pain-like features (e.g., paw shaking or guarding) (*22*, *23*), we used high-speed videography to capture subsecond paw movements at the onset of stimulation (Fig. 6C). Following 0.4-g von Frey stimulation, ELT mice exhibited enhanced paw withdrawal responses, displaying prolonged paw shaking/guarding and increased paw distance traveled (Fig. 6, D to F; fig. S10, F to H; and movie S1). These findings suggest that ELT induces heightened mechanical sensitivity, reflecting an increased pain state.

Pain can disrupt social interactions by provoking irritability or aggression, often as a defensive reaction (*27*). We therefore reasoned that heightened pain states in ELT mice contribute to their aggressive behavior. To test this, we examined whether pharmacological pain relief could attenuate ELT-induced aggression (Fig. 6G). Vehicle treatment had no significant effect on aggression during RI tests, while CAR treatment led to a mild reduction in attack duration. Notably, GBP administration reduced both the duration and frequency of attacks and increased attack latency compared to baseline levels before drug treatment (baseline 1) or after drug washout (baseline 2) (Fig. 6, H to J, and fig. S10I). These effects occurred with no accompanying changes in locomotion (fig. S10J), suggesting that the increased pain state in ELT mice is a key component driving their heightened aggression.

Because $Ca_v1.2$ in the RE contributes to increased susceptibility to aggression and self-harm in ELT mice (Fig. 2), we next examined the functional role of $Ca_v1.2$ in ELT-induced mechanical hypersensitivity. We bilaterally injected AAV5-Cre into the RE of control and ELT *Cacna1c*$^{flox/+}$ or *Cacna1c*$^{flox/flox}$ littermates. ELT *Cacna1c*$^{flox/flox}$ mice in which *Cacna1c* was selectively disrupted in the RE, exhibited normalized mechanical sensitivity, whereas ELT *Cacna1c*$^{flox/+}$ mice showed the expected increase in paw withdrawal responses to a range of von Frey filaments (Fig. 6, K and L). These results indicate that $Ca_v1.2$ in the RE is required for ELT-induced hypersensitivity to mechanical stimuli, which likely contributes to the elevated aggression and self-harming behavior observed in ELT mice.

Furthermore, given our previous data showing that increased vGlut2 RE➔vCA1 circuit activity encodes negative emotional states, which commonly comorbid with pain, we next asked whether inhibiting this pathway could alleviate mechanical hypersensitivity in ELT mice. After injecting either AAV-DIO-enhanced Natronomonas pharaonis halorhodopsin 3.0 (eNpHR3.0)-eYFP or AAV-DIO-eYFP into the RE of control or ELT vGlut2-Cre mice, we implanted optic cannulae over the vCA1 (Fig. 6M). Mice were then subjected to von Frey test under 589-nm light stimulation to assess paw withdrawal thresholds. Optogenetic inhibition of vGlut2 RE➔vCA1 neuronal terminals reduced mechanical hypersensitivity in ELT mice to levels comparable to controls (Fig. 6, N and O). Together with our prior data, these results support the hypothesis that vGlut2 RE➔vCA1 circuit is necessary for the heightened pain sensitivity, which, in turn, increase the risk of related maladaptive behaviors in ELT mice.

RE➔vCA1 neurons separately control aggression and self-harm via distinct efferent targets

Previous studies identified two discrete subsets of vCA1 neurons projecting to either the BA (vCA1➔BA) or the Hypoth (vCA1➔Hypoth) (*60*, *61*). Given that vCA1 receives substantial input from the RE (*62*), we sought to delineate two potential circuit organizations: RE➔vCA1➔BA and RE➔vCA1➔Hypoth. First, to validate distinct vCA1 neuronal subpopulations projecting to BA or Hypoth, we injected AAVretro-Cre into either the BA or Hypoth of C57BL/6 mice, while also injecting AAV-DIO-EGFP into vCA1. This approach allowed us to label only vCA1 neurons projecting to the injection site of AAVretro-Cre—either the BA or Hypoth (Fig. 7, A and C). After examining axonal fibers originating from vCA1➔BA or vCA1➔Hypoth neurons, we found that cells projected primarily to their respective targets but less likely to both (Fig. 7, B and D), consistent with prior studies (*60*). Notably, within the vCA1➔Hypoth pathway, dense vCA1 axonal terminals were observed in discrete hypothalamic subregions, including the lateral hypothalamus (LH), VMH shell, and ventrolateral VMH (VMHvl) (Fig. 7, C and D), which have been implicated in social aggression (*44*, *45*, *63*).

Next, we determined whether both vCA1➔BA and vCA1➔Hypoth neurons receive inputs from the RE using projection-specific transsynaptic tracing (*64*). First, we injected AAVretro-Cre into either the BA or Hypoth and Cre-dependent AAVs expressing avian tumor virus A (TVA) receptor with an optimized rabies glycoprotein (AAV-FLEX-TVA-GFP-oG) into vCA1. Two weeks later, we delivered envelope protein A (EnvA)-pseudotyped, glycoprotein-deleted rabies virus (EnvA-RVΔG-mCherry) into vCA1 to map the monosynaptic inputs to these two populations (fig. S11, A and D). Quantification of mCherry-labeled neurons in the RE revealed that both vCA1➔BA and vCA1➔Hypoth neurons predominantly received inputs from the rostral RE, rather than the caudal RE (fig. S11, A to F). Together, these data establish the existence of two distinct three-node pathways: RE➔vCA1➔BA and RE➔vCA1➔Hypoth.

Amygdala subnuclei have emerged as important sites for the emotional affective dimension of pain (*65*, *66*), while the Hypoth, particularly the VMH, is thought to be a key region of aggression (*44*). We therefore reasoned that two distinct RE➔vCA1➔BA and RE➔vCA1➔Hypoth pathways may differentially regulate self-harming behaviors associated with pain and aggression. To investigate this, we injected an anterograde transsynaptic AAV1-Cre into an upstream node, RE, while a retrograde AAV carrying Flp was injected into either of the downstream targets, BA or Hypoth. Concurrently, we injected AAV-Cre-On and Flp-On (Con/Fon)-ChR2-eYFP or AAV-Con/Fon-eYFP into the middle node, vCA1, followed by optic fiber implantation at the same site. This combination of viral injections allowed selective ChR2 expression in the subsets of vCA1 neurons that receive inputs from the RE and project to either the BA or the Hypoth (Fig. 7E).

In control mice, optogenetic activation of vCA1 neurons specifically relaying between the RE and the BA potentiated both

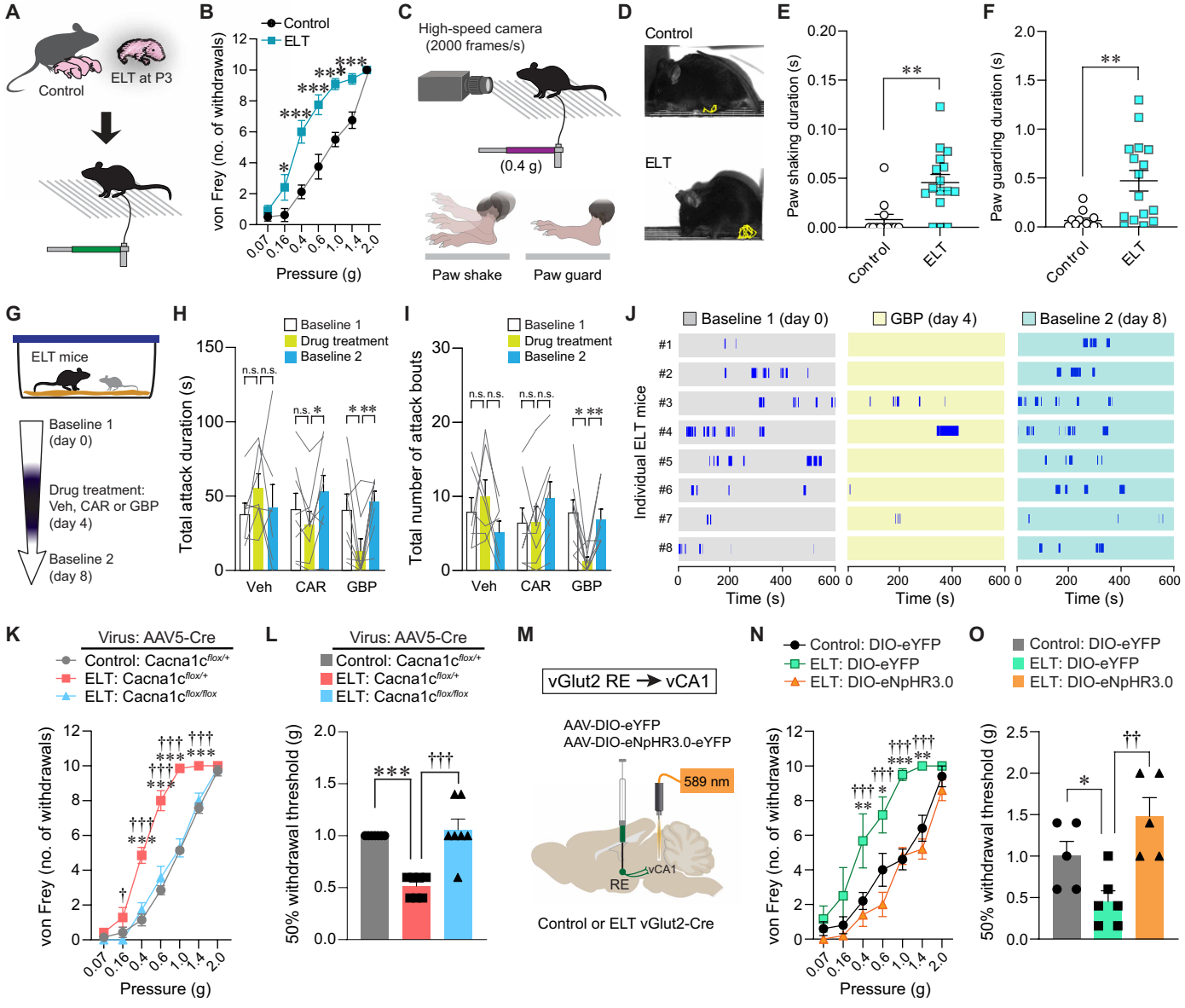

Fig. 6. vGlut2 RE→vCA1 activity is necessary for mechanical hypersensitivity of ELT mice. (**A**) Schematic of von Frey testing after ELT procedure. (**B**) ELT mice exhibited mechanical hypersensitivity with increased number of paw withdrawals in response to 10 stimulations with von Frey filaments ($n = 8$, 12 mice). (**C**) Schematic of high-speed camera setup to capture paw shake or paw guard during 0.4-g von Frey stimulation. (**D**) Representative paw movement trajectories from mice shown in (C), with yellow lines indicating paw tracking. (**E** and **F**) ELT mice showed increased paw shaking and paw guarding ($n = 12$ and 16 mice). (**G**) Experimental timeline for testing the effects of CAR or GBP on ELT-induced aggression. (**H** and **I**) GBP treatment ($n = 8$ ELT mice) significantly reduced attack duration and number. Vehicle ($n = 7$ ELT mice) or CAR treatment ($n = 8$ ELT mice) had no or only mild effects. (**J**) Raster plots showing attack bouts from individual ELT mice during a series of RI tests. (**K**) Mechanical sensitivity of control or ELT *Cacna1c*$^{flox/+}$ and *Cacna1c*$^{flox/flox}$ mice received AAV5-Cre into the RE during von Frey test ($n = 7$, 7, and 7 mice). (**L**) Withdrawal threshold of animals shown in (K). (**M**) Schematic illustrating optogenetic inhibition of vGlut2 RE→vCA1 neurons. (**N**) Mechanical sensitivity of mice expressing eNpHR3.0 or eYFP during von Frey testing with 589 nm of light exposure ($n = 5$, 6, and 5 mice). (**O**) Withdrawal threshold of animals from (N). Statistical analyses with significance: two-way RM ANOVA [(B), (K), and (N)], two-tailed paired *t* test [(E) and (F)], one-way RM ANOVA [(H) and (I)], and one-way ANOVA [(L) and (O)]; $^{*}P < 0.05$; $^{**}P < 0.01$; $^{***}P < 0.001$; $^{\dagger}P < 0.05$; $^{\dagger\dagger}P < 0.01$; $^{\dagger\dagger\dagger}P < 0.001$. Data are presented as means ± SEM.

mechanical sensitivity and Bay K–induced self-harming behavior, whereas the same activation of vCA1 neurons relaying between the RE and the Hypoth did not affect these behaviors (Fig. 7, F and G, and fig. S11, G and H). Instead, optogenetic activation of vCA1 neurons relaying between the RE and the Hypoth preferentially elicited aggressive behaviors, significantly reducing attack latency and increasing attack duration/frequency, whereas a similar activation of the vCA1 neurons between RE and BA did not (Fig. 7, H to J). These data suggest that activation of the RE→vCA1→BA circuit is sufficient to potentiate Bay K–induced self-harm associated with pain, while the activation of the RE→vCA1→Hypoth circuit more selectively triggers aggression.

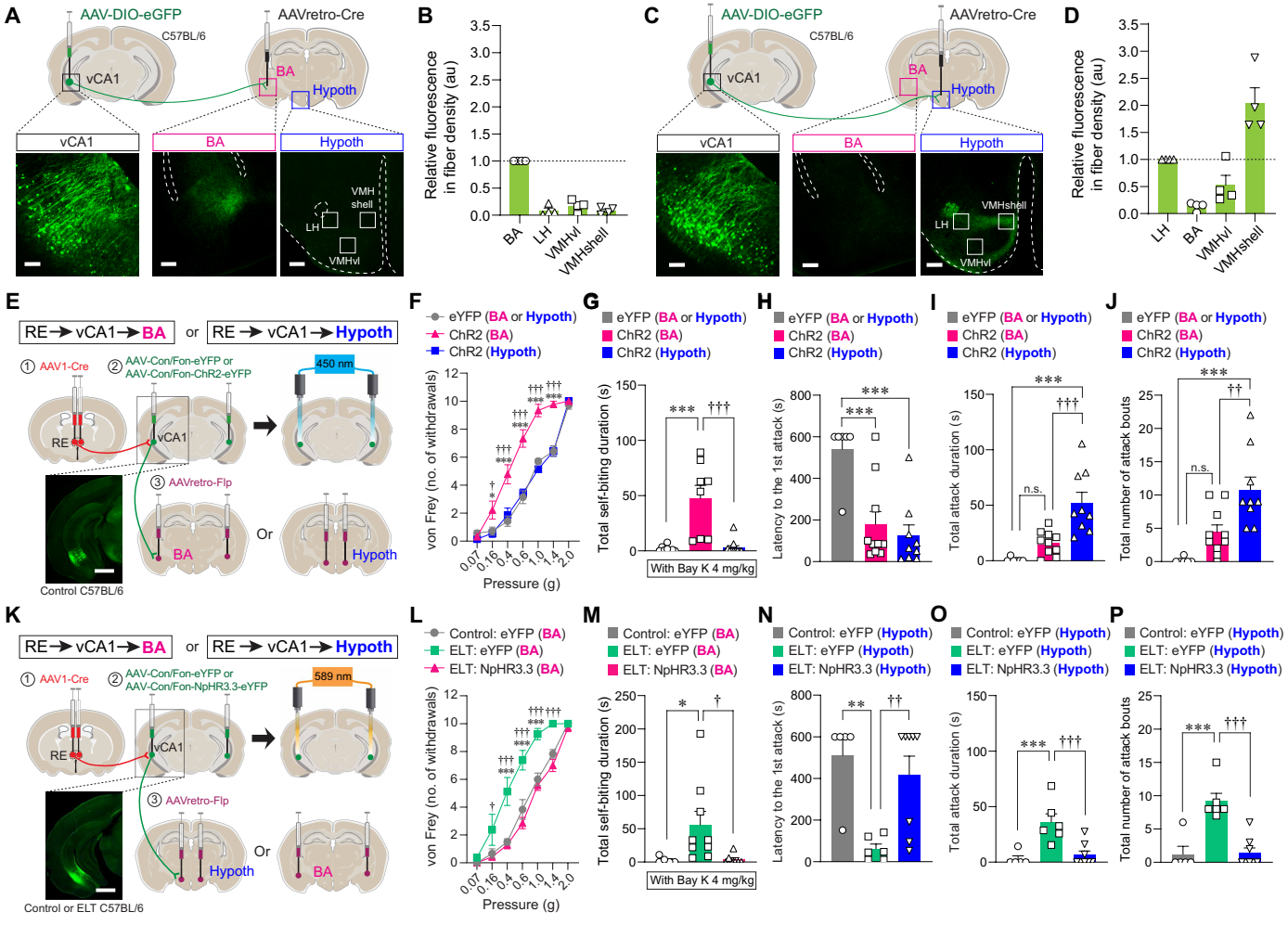

Fig. 7. Dissociable roles of vCA1 neuronal circuits in regulating aggression and self-harm. (**A** and **C**) AAV-DIO-EGFP was injected into the vCA1 and AAVretro-Cre was injected into either the BA (A) or Hypoth (C) of C57BL/6 mice. Images of EGFP-labeled cell bodies in the vCA1 and fibers in the BA and Hypoth. Scale bars, 100 μm (vCA1) and 200 μm (BA and Hypoth). (**B** and **D**) Quantification of fiber density from vCA1➔BA (B) or vCA1➔Hypoth neurons (D) ($n = 4$ mice). (**E** and **K**) Schematic for optogenetic activation (E) or inhibition (K) of input-output–specific vCA1 neuronal subsets. Images show the subset of vCA1 neurons expressing ChR2-eYFP (E) or NpHR3.3-eYFP (K). Scale bars, 1 mm. (**F** and **G**) ChR2-mediated activation of a middle node in the RE➔vCA1➔BA circuit increased mechanical sensitivity (F) ($n = 7$, 9, and 7 mice) and Bay K–induced self-biting behaviors (G) ($n = 8$, 8, and 11 mice). (**H** to **J**) ChR2-mediated activation of a middle node in the RE➔vCA1➔Hypoth enhanced aggressive behaviors ($n = 6$, 10, and 9 mice) with a shortened attack latency and increased attack duration and number. (**L** and **M**) NpHR3.3-mediated inhibition of a middle node in the RE➔ vCA1➔ BA circuit alleviated ELT-induced mechanical hypersensitivity (L) ($n = 6$, 8, and 7 mice) and self-biting behaviors (M) ($n = 5$, 9, and 7 mice). (**N** to **P**) NpHR3.3-mediated inhibition of a middle node in the RE➔vCA1➔Hypoth circuit mitigated aggressive behaviors in ELT mice ($n = 5$, 6, and 8 mice), including an increased attack latency and decreased attack duration and number. Statistical analyses with significance: two-way RM ANOVA [(F) and (L)] and one-way ANOVA [(G) to (J)] and [(M) to (P)]; $^{*}P < 0.05$; $^{**}P < 0.01$; $^{***}P < 0.001$; †$P < 0.05$; ††$P < 0.01$; †††$P < 0.001$. Data are presented as means ± SEM.

This prompted us to examine whether the inhibition of these three-node circuits could restore the maladaptive behavioral characteristics of ELT mice. Using ELT C57BL/6 mice, we used the same intersectional optogenetic strategies described above but injected AAV-Con/Fon-NpHR3.3-eYFP instead of AAV-Con/Fon-ChR2-eYFP (Fig. 7K). Silencing the middle node of the RE➔vCA1➔BA circuit in ELT mice ameliorated the heightened sensitivity to mechanical stimuli during von Frey testing and reduced exacerbated self-harm after submaximal Bay K injection (Fig. 7, L and M, and fig. S11I). On the other hand, inhibition of the RE➔vCA1➔Hypoth circuit significantly attenuated the elevated aggression seen in ELT mice (Fig. 7, N to P). Together, these data support the idea that maladaptive hyperactivity in RE➔vCA1 circuits underlies both aggression and self-harm associated with pain, while the specific behavioral outcome is preferentially determined by the different downstream target of vCA1, either the Hypoth or the BA, respectively.

DISCUSSION

Here, we found that LTCCs in the vGlut2 RE➔vCA1 circuit are shared components underlying both aggression and self-harm. Excessive LTCC activity in vGlut2 RE neurons and the consequent activation of vGlut2 RE➔vCA1 neurons are essential for increasing susceptibility to aggression and self-harm, while silencing vGlut2 RE➔vCA1 neurons restores the levels of these maladaptive behaviors in ELT mice. Furthermore, two distinct downstream targets of

the vCA1— the Hypoth and BA—are key processing nodes for RE-derived information that trigger aggression and self-harm, respectively.

Accumulating evidence indicates a strong association between aggression and self-harm, with a high likelihood of co-occurrence in the same individuals (*4*–*7*), yet the underlying neural mechanisms remain unknown. In this study, we demonstrated that pharmacological activation of LTCCs can induce aggression and self-harm in a dose-dependent manner (Fig. 1). Low-dose Bay K (<0.1 mg/kg, sc) elicited aggression toward conspecifics, whereas high-dose Bay K (>8 mg/kg, sc) triggered self-biting behaviors in mice. RE-specific Bay K administration reproduced these behaviors, promoting aggression at low doses (<2.5 μg per side) and inducing self-harm at high doses (>25 μg per side). These results identify the RE as a common neural substrate mediating both aggression and self-harm and suggest that the extent of RE LTCC activation determines whether mice exhibit aggression or self-harm.

Notably, we found that both low- and high-dose Bay K treatment induced pain-related behavioral responses. At a low dose (0.1 mg/kg, sc), a condition previously shown to trigger aggression, Bay K sensitized pain-like behavioral features, such as paw guarding, in response to mechanical stimuli (fig. S1). Following high-dose Bay K administration, mice exhibited increased facial grimacing, an indicator of spontaneous pain, that preceded or coincided with self-biting behaviors. These findings suggest that Bay K may drive aggression or self-harm as maladaptive strategies for coping with pain. Consistent with this, previous studies have shown that heightened pain states can enhance the perception of social cues as threatening, thereby promoting aggression as a defensive strategy (*26*, *27*, *67*). Furthermore, individuals with chronic pain conditions, such as fibromyalgia or rheumatoid arthritis, are often at a higher risk of self-harm, potentially because "self-inflicted pain" can temporarily relieve the original pain by providing a competing sensory input (*68*–*71*). Future investigations into the role of RE-specific LTCCs in pain processing will further our understanding of the neural mechanisms that transduce pain onset into an increased risk of aggression and self-harm.

ELT is a shared risk factor for the development of aggression and self-harm later in life. Our findings demonstrate that adult mice exposed to ELT paradigm (e.g., pup-dam/littermate separation) exhibit a heightened pain state that inherently potentiates levels of both aggression and self-harm (Fig. 6). Notably, increased LTCC expressions in vGlut2 RE neurons emerged as a key molecular signature in ELT mice, while RE-specific *Cacna1c* deletion effectively reversed the observed maladaptive behaviors—aggression, self-harm, and heightened mechanical sensitivity (Figs. 2 and 6). These findings identify RE-targeted $Ca_v1.2$ modulation as a potential therapeutic strategy for mitigating aggression and self-harm induced or exacerbated by enhanced pain perception, particularly after early adversity.

LTCCs are known to maintain long-lasting activation due to their slower inactivation kinetics, which allows them to facilitate sustained intracellular Ca^{2+} signaling (*55*). In addition, Bay K binds to the α_1 pore-forming subunit of the LTCCs, prolonging the channel's opening time (*72*). Given our vTRAP analysis indicating elevated ribosome-bound mRNA levels of LTCCs in the vGlut2 RE neurons of ELT mice (Fig. 2), we speculated that these neurons exhibit even more sustained Ca^{2+} influx in response to the Bay K stimulation compared to controls. We found that in vivo vGlut2 RE neuronal activity in ELT mice remained active for longer than those of control mice, after submaximal doses of Bay K administration (Fig. 4). Given that self-biting behaviors predominantly occurred during this phase of sustained in vivo vGlut2 RE neuronal activation in ELT mice, it is plausible to think that persistent RE neuronal activation—potentially driven by ELT-induced excessive LTCC activity—is critical for the initiation of self-biting behavior.

In control mice encountering a novel social stimulus, in vivo vGlut2 RE neuronal activity showed a distinctive sharp peak–and–suppression pattern, with an initial activity peak occurring at the first contact with a conspecific stranger, followed by a rapid suppression of that activity (Fig. 3). This dynamic response suggests that vGlut2 RE neurons encode the initial social cue processing, while their activity is quickly suppressed during normal social investigation, likely to prevent excessive engagement with or reaction to social stimuli. Previous studies indicated that γ-aminobutyric acid (GABA)–releasing neurons in the reticular nucleus of the thalamus, ventromedial thalamic nucleus, and ZI send short-range inhibitory projections into the RE (*41*, *73*). Thus, it is plausible that these inputs exert rapid inhibitory control over vGlut2 RE neurons following initial social contact, ensuring naturalistic social interactions.

In contrast, we found that ELT mice exhibited persistent in vivo vGlut2 RE neuronal activity, characterized by a blunt peak–and–no suppression pattern. This sustained neuronal activity potentially contributes to increasing baseline aggression in ELT mice, since optogenetic activation of vGlut2 RE neurons alone was sufficient to induce these behaviors in control mice (fig. S7). Because of the upregulation of LTCC mRNA expression in ELT vGlut2 RE neurons (Fig. 2), it is possible that excessive LTCC activity weakens inhibitory controls on these neurons, allowing their persistent activation. Furthermore, previous studies suggested that RE receives glutamatergic inputs from the mPFC and anterior cingulate cortex (ACC) (*21*, *73*). These input sources may be responsible for driving the initial peak of vGlut2 RE neuronal activation at the onset of first social contact. Future studies examining whether ELT disrupts mPFC➔vGlut2 RE or ACC➔vGlut2 RE circuit activity and impairs the initial cognitive processing of social information will provide important insight into the synaptic and circuit adaptations that underlie impulsive aggression following early adversity.

We also found that activation or inhibition of vGlut2 RE➔vCA1 neurons aggravated or alleviated aggression and self-harm (Fig. 5). In a more naturalistic setting, without social stimuli or Bay K treatment, optogenetic activation of vGlut2 RE➔vCA1 neurons signaled negative valence, triggering avoidance or anxiety-like behaviors (fig. S9). Negative emotions such as anxiety can create social threat bias, often triggering aggressive behaviors (*46*). Self-harm also emerges as a maladaptive coping response to overwhelming emotional distress under mentally or physically challenging situations (*71*). Therefore, vGlut2 RE➔vCA1 neurons may play a role in integrating their negative valence signals with social information, driving aggression toward conspecifics. For mice treated with Bay K treatment, these neurons seem to amplify self-harm by reinforcing negative emotional states.

Our data revealed that the RE sends inputs into two discrete subsets of vCA1 neurons projecting to either the Hypoth or BA. Notably, these two downstream targets are important for driving aggression and self-harm, respectively (Fig. 7). Since the Hypoth, particularly its VMH region, is well recognized for its role in initiating aggressive behaviors (*44*, *45*), it may partake in processing aggression-related information relayed from the RE-to-vCA1 circuit. The BA has been implicated in modulating the affective motivational dimensions of pain (*65*), which may play a crucial role in adjusting the threshold for the induction of self-biting behaviors. Together, our work highlights

the RE as a critical neural hub for integrating aggression- or self-harm–related information, which is then transmitted to vCA1. The vCA1 projections ultimately shape behavioral outcomes depending on whether they target the Hypoth or BA—previously established mechanistic substrates for aggression or affective pain, respectively.

In conclusion, we have delineated distinct LTCC-expressing RE circuits that govern aggression and self-harm, as divergent outcomes along a shared pain-related behavioral continuum. LTCCs within the RE circuitry also provide a mechanism through which ELT sustains vGlut2 RE neuronal activation, enhancing susceptibility to these maladaptive behaviors. This study advances our understanding of how traumatic early-life experiences modify RE neural circuits, leading to long-term behavioral consequences—such as heightened aggression and self-harm—that may arise from pathological pain sensation. Our findings offer a crucial entry point for circuit-based studies in outward or self-directed destructive behavioral symptoms, which remain challenging yet important issues in psychiatric and pain research.

MATERIALS AND METHODS

Animals

All mice were group housed under a 12-hour light/dark cycle in a temperature- and humidity-controlled room with ad libitum access to food and water. C57BL/6J (stock no. 000664), vGlut2-Cre (stock no. 016963), and heterozygous *Cacna1c*^{tm3Hfm}/J (*Cacna1c*$^{flox/+}$; stock no. 024714) mice were obtained from the Jackson Laboratory. vGlut2-Cre mice were crossed with C57BL/6J mice to generate experimental mice. *Cacna1c*$^{flox/+}$ mice were initially crossed with C57BL/6J to yield heterozygous breeders, which were then intercrossed for the generation of homozygous *Cacna1c*$^{flox/flox}$ littermates. Each of the genotypes was determined by PCR analysis. All experiments were conducted with 7- to 9-week-old mice during the light cycle, and age-matched littermates were randomly assigned to each group. Male mice were used in RI test, whereas the initial assessment included both male and female mice (Fig. 1, A to D). For other behavioral experiments, vTRAP, qPCR, FISH, and anatomical tracing, a similar number of both male and female mice were used. All experimental protocols were approved by the Institutional Animal Care and Use Committee of the Virginia Polytechnic Institute and State University (#23-008).

ELT procedures

The generation of ELT mice followed previously established methods (*48*, *74*). Briefly, pregnant female mice were housed individually from gestational days 14 to 16. Between P3 and P4, ELT pups were separated from their dam and littermates for 23 hours. During this period, they were individually placed in partitioned small chambers with bedding and maintained in an incubator at 32° ± 1°C. After the separation, ELT pups were reunited with their dam and littermates, whereas control pups remained undisturbed in the maternal nest. All pups were weaned at P21 and subsequently housed in groups of three to five of the same sex until the start of the experiments.

RI test

The RI tests were carried out as previously described with minor modifications (*75*, *76*). Each experimental mice ("residents") was group housed in a home cage with unchanged bedding for at least 1 week before the experiments. On the test day, the mice were acclimated to the testing room for 1 hour in their home cages. The cagemates were temporarily moved to a holding cage, and the experimental mouse was allowed to explore its home cage freely for 10 min (habituation). A novel, same-sex juvenile C57BL/6 mouse (4 to 5 weeks old, "intruder") was then introduced into the home cage of the resident, and mice were allowed to freely interact for 10-min test session. All behaviors were video recorded using a top-view camera (Logitech) and analyzed by two experimenters who were blind to the test conditions. Behavioral analysis was conducted using Adobe Premiere Pro 2024 software. Attack bouts were identified through frame-by-frame analysis and were defined as frames in which the resident mouse engaged in biting or intense aggressive behavior immediately following a biting episode. To quantify aggressive behavior, the latency to the first attack, total attack duration, and the number of attack bouts in each test session were recorded.

To test the effects of analgesics on aggression, a series of RI tests were conducted. Baseline aggression levels were first assessed on day 0 (baseline 1). On day 4, mice were subjected to RI tests 1 hour after administration of CAR (5 mg/kg, sc) or GBP [100 mg/kg, intraperitoneally (ip)]. To confirm the recovery of aggression after drug washout, the same mice were retested on day 8 (baseline 2). A novel intruder was introduced in each testing session to avoid habituation effects.

Self-biting behavior analysis and wound scoring

To induce self-biting behavior, Bay K was administered either subcutaneously (4 or 8 mg/kg, sc) or intracranially (25 μg/0.5 μl per side). Immediately after the injection, each mouse was placed in a transparent acrylic chamber (6.5 cm by 6.5 cm by 6.5 cm). Using multicamera setup (Open Broadcaster Software, V30.1.2), all behaviors were recorded for 40 min with three cameras (Logitech): one for a bottom view and two for each side view. Self-biting behavior was defined as a repetitive gnawing and biting motion directed at various body regions, including the fore/hind paws, chest, shoulder, and tail, initiated when the mouth contacts these areas. Two blinded experimenters manually recorded the duration of self-biting episodes. Adobe Premiere Pro 2024 software was used for frame-by-frame analysis to identify the defined self-biting behaviors, not including grooming behaviors characterized by licking motions directed at body surfaces. After 40-min video recording, each mouse was visually examined for wounds across body regions. The severity of injuries was scored on the basis of criteria adapted from previous studies (*77*) with minor modification: score 0, no visible tissue damage; score 1, mild redness on bitten nails and toe tips without skin damage; score 2, superficial abrasions, including peeled or frayed skin in multiple sites, but no active bleeding; score 3, pronounced redness and swelling with visible blood traces; score 4, severe tissue injury including digit amputation, deep lesions, and unrecognizable paw area.

For self-harm tests involving chewable items, either a nylabone chew toy or a wooden block was placed in the acrylic chamber at the onset of video recording for both vehicle- or Bay K–injected mice. To assess the effects of Bay K on appetitive behaviors, these mice were presented with either a high-fat diet (60% kcal fat; D12492, Research Diets) or a same-sex, age-matched social stimulus in their homecage for 40 min.

Mouse grimace scale

The MGS scoring was performed as previously described (*30*), with minor modifications. Briefly, Bay K (0.1, 4, or 8 mg/kg, sc) or vehicle

was injected 10 min before placing each mouse in a stainless/aluminum imaging chamber (5.5 cm by 14 cm by 6 cm). To test the effects of analgesics on Bay K–induced increases in grimace scores, mice received CAR (5 mg/kg, sc) or GBP (100 mg/kg, ip) 10 min before Bay K injection. During a 30-min video recording, a Canon Vixia HF R9700 camera was placed 80 cm from the front side of the imaging chamber, which remained open to the air to prevent glare and reflections. The light-emitting diode (LED) strip light (3200 to 6500 K; Waveform Lighting, Vancouver, WA, USA) was placed above the chamber for illuminating the mouse's face (~1000 lux).

For MGS analysis, each 30-min video recording (1920 × 1080 red, green, and blue, 30 frames/s) of C57BL/6 mice was evaluated by PainFace, a cloud-based software platform (http://painface.net) at 1 frame/s with build 2022.11.15. The software detected four FAUs of MGS: (i) orbital tightening, contraction of the muscles around the eyes, causing partial eye closure; (ii) ear position, ears pulled back and flattened against the head with the base of the ears becoming more horizontal or retracted; (iii) nose bulge, muscular contraction around the nose, making it appear more pronounced or swollen; and (iv) whisker change, whiskers becoming stiff and drawn closer to the face or pulled back. Each FAU was automatically scored on a three-point scale of "0" (not present), "1" (moderate), or "2" (obvious). Total MGS score was calculated as the sum of the scores from all four FAU, ranging from 0 to 8. The percentage of frames that were scored throughout the 30-min session was categorized into three MGS severity bins: low (0 to 2), medium (3 to 4), and high (5 to 8).

Rearing and audible vocalization measurement

Following administration of either vehicle or Bay K (4 or 8 mg/kg, sc), each mouse was placed in a transparent acrylic chamber (6.5 cm by 6.5 cm by 6.5 cm). Mouse behaviors and audible vocalizations (squeaks) were recorded by cameras for 40 min and analyzed by two blinded experimenters. The numbers of rearing instances and audible calls during the session were manually recorded. Rearing was defined as vertical posture in which the mouse stood on its hind legs, either unsupported or with its forepaws resting against the chamber walls.

Locomotion

The locomotion test was conducted in an open-field arena (44 cm by 44 cm by 44 cm). Mice were individually placed in the arena and allowed to move freely for 60 min. Their activity was monitored by a camera (Logitech) positioned above the arena and analyzed using tracking software (Viewer 3.0, BIOBSERVE).

Open field test

Each mouse was placed in the open-field arena (44 cm by 44 cm by 44 cm) and allowed to explore freely for 10 or 15 min. The open-field arena was subdivided into two zones: a center zone (20 cm by 20 cm) and a periphery zone. The movement of mice was monitored with a camera (Logitech) and analyzed by tracking software (Viewer 3.0, BIOBSERVE).

Elevated plus maze

The elevated plus maze consisted of two open arms, two closed arms, and a center platform, elevated to a height of 30.5 cm above the ground. Mice were placed in the center and allowed to explore the maze for 5 min. The movement of the mice was recorded using a camera mounted above the arena and analyzed using tracking software (Viewer 3.0, BIOBSERVE).

Restraint stress

Mice were individually placed in rodent immobilization bags (Harvard Apparatus) that restricted movement while allowing normal respiration. Each mouse underwent restraint for 6 hours in a quiet and dimly lit room to minimize exposure to additional stressors.

Serum corticosterone measurement

Mice were anesthetized with isoflurane and decapitated either at baseline or 0.5 hours after restraint stress. Whole-trunk blood samples were collected in 1.5-ml microcentrifuge tubes and allowed to clot at room temperature for 30 min. Tubes were then spun at 3000*g* for 15 min at 4°C. Supernatant containing clear serum was stored at −80°C until an enzyme-linked immunosorbent assay was applied to measure serum corticosterone using an assay kit (EIACORT, Invitrogen).

Von Frey test

Mice were habituated for 30 min in rectangular plexiglass chambers placed on an elevated mesh floor. A series of seven von Frey filaments (ranging from 0.07 to 2 g; Stoelting) were applied to the plantar surface of the hind paw in ascending order, starting with the lowest force. Each filament was applied until it bent, with a 5- to 10-s interval between successive stimulations. Each filament was tested 10 times, and the number of paw withdrawal responses was recorded. The withdrawal threshold was determined as the lowest filament that elicited a withdrawal response in at least 5 of 10 trials (≥50% of trials).

Hot plate test

Thermal sensitivity was evaluated using the hot plate test. Mice were placed on a metal surface heated to 53.5°C, which is enclosed within an acrylic container (Ugo Basile). Latency to the first nocifensive response, paw flinching, licking, or jumping, was measured. All testing was conducted by experimenters blinded to drug treatment conditions.

High-speed videography and PAWS data analysis

High-speed imaging and automated analysis of paw withdrawal behavior were performed as previously described (*24*, *25*), with minor modifications. Mice were habituated for 30 min in rectangular plexiglass chambers on a mesh platform. A high-speed camera (Photron FASTCAM Mini AX50, Zeiss 2/100M ZF.2 lens) was positioned at ~3 feet (91.44 cm) with 10° angle from the plexiglass chambers to capture paw movements at 2000 frames/s for up to 1.75 s following application of a 0.4-g von Frey filament to the hind paw.

For markerless pose estimation, 20 frames were randomly selected from each recorded videos through SLEAP toolbox and manually annotated for toe, center, heel, and two reference points on the plexiglass chamber (top and bottom right corner). These labeled frames were used to train a pose estimation model using SLEAP. The trained model was applied to the full video dataset to track the toe, center, and heel. Data points with tracking confidence below 80% were excluded and replaced with interpolation. A rolling average filter was applied to smooth the data. Tracking confidence was highest for the center point, which was used for all subsequent analyses. These tracking data were analyzed using PAWS (*22*, *23*, *25*), which extracted features such as guarding and shaking durations, paw distance traveled, and the number of paw shakes. To generate trajectories, we overlaid the inferred x and y positions of the paw center in each video frame on a single still image corresponding to the mouse's paw during the tests.

Drug treatment

For subcutaneous or intraperitoneal injections, Bay K (Sigma-Aldrich) was dissolved in sterile distilled water containing 1.6% dimethyl sulfoxide (DMSO), 4% ethanol, and 4% Tween 80. To measure self-biting/self-injurious behaviors, rearing, audible vocalization, and locomotion, Bay K (0.1, 4, or 8 mg/kg, sc) was injected immediately before the experiment. For testing self-biting/self-injurious behaviors with analgesics, CAR (5 mg/kg, sc; Zoetis) and GBP (100 mg/kg, ip; Sigma-Aldrich) were dissolved in sterile distilled water and injected to mice 10 min before Bay K administration. For RI, von Frey, and hot plate tests, mice were treated with Bay K (0.01 or 0.1 mg/kg, sc) 30 min before testing. For c-fos immunostaining, mice were perfused 1 hour after administrations of either vehicle or Bay K (4 mg/kg, sc).

For intracranial injections, a 30-gauge internal cannula (RWD Life Science Inc.), extending 0.2 mm beyond the guide cannula, was connected to a 1-μl Hamilton syringe via polyethylene-20 tubing. Drugs were bilaterally microinjected into the target brain regions over 30 s, and the cannulas were left in place for an additional 1 min to ensure adequate diffusion. For locomotion, OFT and RI tests, Bay K (0.25 or 2.5 μg/0.5 μl per side) was infused 1 hour before testing. For assessing self-biting/self-injurious behavior, Bay K (2.5 μg/0.5 μl per side) was administered 5 min before video recording. Nicardipine (1 or 5 μg/0.5 μl per side; Sigma-Aldrich) was dissolved in DMSO and bilaterally infused into the RE 1 hour before locomotion, RI testing, or systemic administration of Bay K (4 mg/kg, sc). For chemogenetic control of vGlut2 RE terminals in the mPFC and vCA1, CNO (1 mM, dissolved in sterile distilled water; 0.5 μl per side) was delivered 5 min before the start of either the RI test or systemic administration of Bay K (4 mg/kg, sc).

Fluorescent in situ hybridization

Mice were deeply anesthetized using isofluorane inhalation and perfused with ice-cold phosphate-buffered saline (PBS). Brains were rapidly extracted and flash frozen with isopentane (Sigma-Aldrich) prechilled with dry ice in 70% ethanol. Coronal brain slices (16 μm) containing the RE were sectioned using a cryostat (CM1860, Leica) and mounted on slides. FISH was performed using the RNAscope Fluorescent Multiplex Assay (Advanced Cell Diagnostics). Slides were fixed in 4% paraformaldehyde (PFA) for 15 min at 4°C and subsequently dehydrated for 5 min with 50, 70, and 100% ethanol at room temperature. Sections were then incubated with a Protease IV solution for 30 min and washed with 1 × PBS before being incubated with probes for 2 hours at 40°C in the HybEZ oven (Advanced Cell Diagnostics). All probes used were commercially available: Mm-*Cacna1c* (445451), Mm-*Cacna1d* (502591), and Mm-*Slc17a6* (vGlut2; 319171). After washing twice with wash buffer, the signals of the tissue sections were amplified in the amplification buffers at 40°C. After the final rinse, 4′,6-diamidino-2-phenylindole (DAPI) solution was applied to the sections. Slides were visualized with a Nikon SoRa inverted spinning disk confocal microscope.

Immunohistochemistry and c-fos quantification

Mice were perfused intracardially with 4% PFA/PBS and postfixed overnight at 4°C. Coronal sections (50 μm) were sliced using a vibratome (VT1000, Leica). Free-floating sections were washed in PBS containing 0.3% Triton X-100 (PBS-T; pH 7.4) and incubated in 1% (v/v) bovine serum albumin in PBS-T for 1 hour. The sections were then incubated overnight with rabbit anti–c-fos antibody (1:5000; #2250, Cell Signaling Technology) or rabbit anti-FLAG antibody (1:1000; #F7425, Sigma-Aldrich) in PBS-T. For $Ca_v1.2$ and $Ca_v1.3$ immunostaining, sections were incubated with rabbit anti-$Ca_v1.2$ (1:250; #ACC-003, Alomone Labs) or rabbit anti-$Ca_v1.3$ (1:250; #ACC-005, Alomone Labs) for 48 hours. The following day, sections were washed in PBS-T and incubated with Alexa Fluor–conjugated secondary antibodies (1:1000; Thermo Fisher Scientific) for 1 hour, washed in PBS, and mounted on slides with DAPI counterstain medium (Thermo Fisher Scientific). Images were acquired using a Nikon SoRa inverted spinning disk confocal microscope and analyzed quantitatively using ImageJ.

For c-fos quantification in the RE, sections were obtained from bregma, −0.58 to −0.94 mm, from each animal. The neurons located from the dorsal edge of the third ventricle up to +0.5 mm dorsally and within ±0.5 mm laterally from the third ventricle were considered part of the RE. Cell counts were made within this defined area by applying consistent thresholds across all images and using the "Analyze Particles" function in Fiji (ImageJ).

Viral translating ribosome affinity purification

The vTRAP assay was conducted as previously described (*51*, *78*) with slight modifications. Briefly, AAV-FLEX-EGFPL10a was bilaterally injected into the RE of vGlut2-Cre mice. Mice were euthanized 3 weeks after the viral injection, and coronal brain slices (250 μm) were prepared in prechilled sectioning buffer containing cycloheximide (0.1 mg/kg) and 100 μM rapamycin in PBS (pH 7.4) using a vibratome (VT1200, Leica). Dissected RE tissue was transferred to prechilled 1.5-ml tubes, snap frozen on dry ice, and stored at −80°C until use. RE tissues from two mice were pooled to create one sample, with five and six replicates per group (Fig. 2N). RE tissue was homogenized in a buffer containing 20 mM Hepes-KOH (pH 7.4), 5 mM $MgCl_2$, 150 mM KCl, 1% NP-40, 1 mM dithiothreitol, cycloheximide (0.1 mg/kg), 0.1 mM rapamycin, ribonuclease inhibitor (#AM2696, Invitrogen), and cOmplete EDTA-free protease inhibitor cocktail (#04693159001, Roche). EGFP-labeled ribosomes were immunoprecipitated using Dynabeads Protein G (#10003D, Thermo Fisher Scientific) precoated with anti-GFP antibodies (#50430-2-AP, Proteintech) (*79*), and bound RNA was purified using the Absolutely RNA Nanoprep Kit (#400753, Agilent). Purified RNA was then reverse transcribed using SuperScript IV first-strand cDNA synthesis kit (Thermo Fisher Scientific) with the Universal Primer 1 (UP1) (5′-ATATGGATCCGGCGCGCCGTCGACTTTTTTTTTTTTT-TTTTTTTTTTTT-3′).

Quantitative real-time polymerase chain reaction

Mice were anesthetized with isoflurane and coronal brain slices (250 μm) were prepared using a vibratome (VT1200, Leica). The RE, mPFC, NAc, LS, VMH, vCA1, or DR was dissected, immediately snap frozen on dry ice, and stored at −80°C until RNA extraction. Total RNA was isolated using the Hybrid-R RNA purification kit (#350-101, GeneAll Biotechnology). Purified RNA was then reverse transcribed using SuperScript IV first-strand cDNA synthesis kit (Thermo Fisher Scientific). Target sequences were amplified using the TaqMan Gene Expression Assay Kit (Thermo Fisher Scientific) and quantified using the QuantStudio 3 Real-Time PCR System (Applied Biosystems). TaqMan probes (Thermo Fisher Scientific) used in the assay included *Cacna1c* (Mm01188822_m1), *Cacna1d* (Mm01209927_g1), *Calb1* (Mm00486645_m1), *Calb2* (Mm00801-461_m1), *Necab1* (Mm00724274_m1), *Tnnt1* (Mm00449089_m1),

and glyceraldehyde-3-phosphate dehydrogenase (*GAPDH*) (Mm99-999915_g1). Relative mRNA expression levels were calculated using the comparative threshold cycle (ΔC_t) method, with GAPDH as the internal control: $\Delta C_t = C_t$ (gene of interest) $- C_t$ (GAPDH). Fold change was calculated by normalizing the value of each sample to the mean of the control samples. Gene expression changes were assessed using the $2^{-\Delta\Delta Ct}$ method, with expression levels normalized to GAPDH and compared to control samples.

Virus generation

AAV vector plasmids were constructed using standard molecular cloning methods or were obtained from external sources. Origins and cloning of AAV-Elongation Factor 1α (EF1α)-DIO-eYFP, AAV-EF1α-fDIO-EGFP, AAV-EF1α-DIO-synaptophysin-smFP-FLAG, AAV-hSyn-DIO-mCherry were described previously (*80*). AAV-FLEX-EGFPL10a (plasmid #98747), AAV-hSyn-DIO-hM3D(G_q)-mCherry(plasmid#44361),andAAV-hSyn-DIO-hM4D(G_i)-mCherry (plasmid #44362) were purchased from Addgene. Briefly, AAV was produced by transfection of 293T cells (#632273, Takara) with three plasmids: AAV vector plasmid expressing the target construct (pAAV), AAV helper plasmid (pHELPER; Agilent), AAV rep-cap helper plasmid (pRC-DJ; gift from M. Kay). At 72 hours after transfection, the cells were harvested and lysed. Next, the viral particles were purified by an iodixanol step gradient ultracentrifugation method. The iodixanol was diluted, and the AAV was concentrated using a 100-kDa molecular mass cutoff ultrafiltration device. The genomic titer was validated by qPCR. The AAV vectors were diluted in 1× PBS to a working concentration of ~10^{12} viral particles/ml.

Stereotaxic surgeries and histology

C57BL/6, vGlut2-Cre, *Cacna1c*$^{flox/+}$, or *Cacna1c*$^{flox/flox}$ mice were anesthetized with a mixture of ketamine (100 mg/kg) and dexmedetomidine (0.5 mg/kg) and then placed in a stereotaxic apparatus (David Kopf Instruments). Body temperature was kept stable using a heating pad (33°C) while recovering from anesthesia. Viral injection targets were determined using coordinates based on the Paxinos and Franklin mouse brain atlas (*81*). For all experiments involving viral expression in the RE, 200 nl of virus was infused into RE [anteroposterior (AP), −0.82; mediolateral (ML), ±0.25; dorsoventral (DV), −4.45] at a slow rate of 75 nl/min to minimize leakage. Preemptive analgesia was administered via injections of buprenorphine (0.1 mg/kg, sc), with postoperative analgesia provided by additional buprenorphine injections.

For microinjections of the Bay K or nicardipine, a guide cannula (26 gauges; RWD Life Science Inc.) was chronically implanted into the RE (AP, −0.82; ML, ±0.25; DV, −4.45), mPFC (AP, +1.78; ML, ±0.4; DV, −2.55), NAc (AP, +1.7; ML, ±0.5; DV, −4.5), LS (AP, +0.85; ML, ±0.4; DV, −3.2), VMH (AP, −1.4; ML, ±0.5; DV, −5.5), vCA1 (AP, −3.8; ML, ±3.25; DV, −4.00), and DR (AP, −4.62; ML, 0; DV, −2.93). Implanted cannulae were secured to the skull with an initial layer of adhesive cement (C&B Metabond, Parkell), followed by a second layer of dental cement (Ortho-Jet, Lang Dental), and then obturators were placed in the guide cannulae. Sterile tissue adhesive (Vetbond, 3M) was used to close the incision. Behavioral tests were performed 2 weeks after the implantation. Upon completion of the experiments, mice were deeply anesthetized and perfused with 4% PFA. Brains were sectioned coronally at a thickness of 50 μm. The sections were stained with 0.2% cresyl violet (Sigma-Aldrich) to verify the placement of the cannula tips. Only data from mice with confirmed placement of the cannula tips in the target areas were included in the final analysis. Mice with off-target implant tip locations were excluded from the final analysis.

For vTRAP assay, AAV-FLEX-EGFPL10a were bilaterally injected into the RE of vGlut2-Cre mice using a Hamilton microsyringe connected to borosilicate glass pipettes at a constant rate controlled by a syringe pump (PHD Ultra, Harvard Apparatus). Mice were given 2 weeks to recover from the virus injections before RE dissection.

For experiments involving the local deletion of *Cacna1c*, AAV5-hSyn-Cre (#105553-AAV5, Addgene) was bilaterally injected into the RE of *Cacna1c*$^{flox/+}$ or *Cacna1c*$^{flox/flox}$ mice. Mice were given 2 weeks for molecular validation and behavioral testing. *Cacna1c* deletion in the RE was examined by qPCR and FISH (Fig. 2).

For in vivo Ca^{2+} imaging experiments, a sterile 26-gauge needle was gradually lowered into the RE of vGlut2-Cre mice (4 to 5 weeks old) to a depth of −3.65 mm from the skull, making a path for GRIN lens implantation. AAV5-DIO-GCaMP6f (#100835-AAV5, Addgene) was then injected into the same RE location at a depth of −4.45 mm. Subsequently, a ProView Integrated GRIN lens (diameter, 0.5 mm; length, 8.4 mm; Inscopix) was implanted 100 μm above the virus injection site. The implanted GRIN lens and microendoscope baseplate were secured to the skull as described above, and a baseplate cover (Inscopix) was used to protect the lens when not in use. In vivo Ca^{2+} imaging tests were performed 4 weeks after the ProView Integrated GRIN lens implantation.

For chemogenetic manipulation of vGlut2 RE terminal activity, vGlut2-Cre mice were bilaterally injected with AAV-DIO-mCherry, AAV-DIO-hM3D(G_q)-mCherry, or AAV-DIO-hM4D(G_i)-mCherry into the RE. Bilateral drug infusion cannulae (26 gauges; RWD Life Science Inc.) were implanted just above the mPFC (AP, +1.78; ML, ±0.4; DV, −2.55) or vCA1 (AP, −3.8; ML, ±3.25; DV, −4.00). Mice were allowed 2 weeks for recovery before behavioral testing.

For optogenetic activation of vGlut2 RE cell bodies, vGlut2-Cre mice were bilaterally injected with AAV-DIO-eYFP or AAV-DIO-hChR2(H134R)-eYFP (#20298-AAV5, Addgene) into the RE. Bilateral optic fibers [200 μm in diameter, 0.66 numerical aperture (NA); Doric Lenses] were implanted into the RE. For control of vGlut2 RE→vCA1 terminal activity, vGlut2-Cre mice were bilaterally injected with either AAV-DIO-eYFP, AAV-DIO-hChR2(H134R)-eYFP, or AAV-DIO-eNpHR3.0-eYFP (#26966-AAV5, Addgene) into the RE, and bilateral optic fibers (200 μm in diameter, 0.66 NA; Doric Lenses) were inserted just above the vCA1 (AP, −3.8; ML, ±3.25; DV, −4.00). For manipulation of vCA1 as a middle node between RE and BA or between RE and Hypoth, AAV1-hSyn-Cre (#105553-AAV1, Addgene) was bilaterally injected in the RE of C57BL/6J, while 350 nl of AAVretro-EF1α-Flp (#55637-AAVrg, Addgene) was bilaterally injected either in the BA (AP, −1.75; ML, ±3.0; DV, −5.5) or Hypoth (AP, −1.65; ML, ±0.65; DV, −5.45). Subsequently, 350 nl of AAV-hSyn-Con/Fon-ChR2-eYFP, AAV-hSyn-Con/Fon-eYFP (gifts from K. Deisseroth; #INTRSECT AAV5&DJ, UNC Vector Core), or AAV-nEF-Con/Fon-NpHR3.3-eYFP (#137152-AAV8, Addgene) was bilaterally injected into the vCA1, followed by implantation of bilateral optic fibers (200 μm in diameter, 0.66 NA; Doric Lenses) just above the vCA1. Implanted fibers were fixed to the skull with adhesive and dental cement, as described above. Mice were allowed 3 weeks for recovery before behavioral testing. Viral injections and cannula/fiber placements were confirmed after the completion of behavioral experiments.

For input-output mapping experiments with EnvA-pseudotyped rabies virus, 350 nl of AAVretro-hSyn-Cre (105553-AAVrg) was

unilaterally infused into either BA (AP, −1.75; ML, ±3.0; DV, −5.5) or Hypoth (AP, −1.65; ML, ±0.65; DV, −5.45) of C57BL/6 mice. Subsequently, 350 nl of AAV8-hSyn-FLEX-TVA-P2A-GFP-2A-oG (Salk Institute Viral Vector Core) was injected into ipsilateral vCA1 (AP, −3.8; ML, ±3.25; DV, −4.00) at a rate of 100 nl/min. After allowing for 2 weeks of viral expression, mice were again anesthetized as previously described, and EnvA-ΔG-rabies-mCherry (Salk Institute Viral Vector Core) was infused into ipsilateral vCA1, using skull scars as anatomical reference points. Mice were euthanized 5 days after the final injection.

For output mapping, AAV-DIO-synaptophysin-smFP-FLAG was unilaterally injected into the RE of vGlut2-Cre mice. To evaluate the extent to which vGlut2 RE➔vCA1 neurons collateralize to different target regions, AAV-fDIO-EGFP was unilaterally injected in the RE, and 350 nl of AAVretro-EF1α-DIO-Flp was injected in the ipsilateral vCA1 of vGlut2-Cre mice. For similar assessments in vCA1➔–BA or vCA1➔Hypoth neurons, 350 nl of AAV-DIO-EGFP was unilaterally injected in the vCA1, and 350 nl of AAVretro-hSyn-Cre was injected in the ipsilateral either BA or Hypoth of C57BL/6 mice. Mice were given 2 weeks to recover from the virus injections before histological analysis. For CTB-mediated tracing, 300 nl of CTB-488 (#C34775, Thermo Fisher Scientific) or CTB-647 (#C34778, Thermo Fisher Scientific) was infused into the unilateral mPFC or vCA1 of C57BL/6J mice. Mice were euthanized 5 days after the CTB injection.

After each experiment, the extent of viral transduction was assessed to determine whether it was restricted to the RE or vCA1 without off-target effects in other adjacent areas. If the viral expression was found outside the desired area or if the viral transduction was insufficient, covering less than 50% of the target area, then the mice were excluded from the final dataset, which was determined by two experimenters blinded to the experimental design. Injection sites were verified in all animals by preparing coronal sections containing the target region, and animals with incorrect injection placements were excluded from the analysis.

In vivo Ca^{2+} imaging

Mice were habituated for 30 min either in their home cage or a transparent acrylic chamber (6.5 cm by 6.5 cm by 6.5 cm) with a head-mounted Inscopix miniature microscope (nVoke 2.0) connected to a commutator to prevent cable entanglement during the experiment. Before data acquisition, scope focus, excitation (EX)-LED power, and gain were optimized for each mouse and remained constant throughout the experiment. To monitor the GCaMP6f fluorescence in response to social or nonsocial stimulus, a conspecific stranger mouse or a fake mouse (mouse-shaped toy) was introduced into home cage after baseline recording. Mice were allowed to investigate each stimulus freely, while GCaMP6f fluorescence was recorded, and the rate of Ca^{2+} transients was measured during 0.5-min periods following the first contact and compared to the rate during a 0.5-min baseline recording. To examine how in vivo activity of individual vGlut2 RE neurons changes after Bay K administration (4 or 8 mg/kg, sc), the rate of Ca^{2+} transients was measured during 1-min periods after Bay K injection and compared over time. All mouse behaviors were recorded simultaneously using video cameras.

In vivo Ca^{2+} imaging data processing and analysis

Inscopix Data Acquisition software (version 1.6.1) was used to acquire TIFF images of fluorescence dynamics at 20 frames/s. The EX-LED power was maintained at 0.9 to 1.4 mW/mm^2 with a gain of 3.5. Inscopix Data Processing software (v 1.6.1) was used to preprocess Ca^{2+} data from each imaging session. Briefly, Ca^{2+} imaging data were down-sampled temporally (2× temporal bin) and spatially (4× spatial bin) and motion corrected for rigid brain movement. Regions of interest corresponding to cell bodies were identified in maximum projection images using an automated cell-finding function and manually inspected to ensure accuracy. Raw fluorescence traces for individual vGlut2 RE neurons were then *z*-normalized using the mean and SD of the entire imaging session. The normalization of individual neuronal Ca^{2+} dynamics was performed using Inscopix Python (v3.8) scripts for further analysis. To detect individual Ca^{2+} transients, $\Delta F/F_0$ values from individual vGlut2 RE neurons were processed using customized MATLAB-based software (MathWorks) to remove slow drifts, estimated by a median filter of 10 s in width (*82*, *83*). The median absolute deviation (MAD) of the entire time series was computed, and Ca^{2+} transients were extracted by identifying upward transients exceeding a 5.5-MAD threshold, with an interval no shorter than 2 s between successive events.

Behavioral events, including the onset of social bouts [e.g., close following (<1 cm), anogenital/body sniffing, mounting, and nose-to-nose contact], physical contact with the fake mouse, and self-biting bouts, were manually scored from recorded videos by two experimenters blinded to the experimental design. To correlate vGlut2 RE neuronal activity with self-biting behaviors, Ca^{2+} transients of from individual neurons were aligned to the first self-biting bout onset. During 2.5-min period following the first self-biting bout, the number of neurons exhibiting Ca^{2+} transients at the onset of self-biting episodes were quantified from ELT mice treated with Bay K (4 mg/kg, sc). The percentage of the correlated or noncorrelated cells was calculated relative to the total number of vGlut2 RE neurons detected during the image session.

For the classification of vGlut2 RE neuronal responses to social or nonsocial contact with the intruder or fake mouse, the baseline Ca^{2+} transient rate and SD (σ) were determined during 4-min period before introducing either a fake mouse or an intruder mouse. Cells were classified as activated if their average Ca^{2+} transient rate during the 0.5-min window at 3 min after the first contact exceeded (baseline Ca^{2+} transient rate + 0.5σ), as inhibited if it fell below (baseline Ca^{2+} transient rate − 0.5σ); and as null if it remained within the range of (baseline Ca^{2+} transient rate − 0.5σ) to (baseline Ca^{2+} transient rate + 0.5 σ).

Optogenetic stimulation

For ChR2-mediated activation, a 3-m-long fiber optic patch cord (200 μm in diameter, 0.57 NA; Doric Lenses) was connected to the chronically implanted optic fiber and positioned above the behavioral testing area. This setup allowed the animals to move freely while being stimulated with 450-nm blue light (20 Hz, 5-ms pulses) for activation. For eNpHR3.0-mediated inhibition, the patch cord was attached to a 589-nm yellow light source (Doric Lenses), with continuous light applied bilaterally to achieve inhibition. The light power at the fiber tip was set to 10 mW for each optic fiber. During RI tests involving optogenetic manipulation, light stimulation began 5 min before introducing the intruder mouse into the home cage. For RI tests with ChR2-mediated activation (figs. S7, C to E, and S9, B to D), each mouse underwent RI tests twice, separated by 48 hours, one session with low-frequency blue light (5 Hz, 5-ms pulses) and one with high-frequency light (20 Hz, 5-ms pulses). The order of low- or high-frequency light stimulation was counterbalanced across groups.

Real-time place test

A 3-m-long fiber-optic patch cord (200 μm in diameter, 0.57 NA; Doric Lenses) was connected to the chronically implanted optic fiber and suspended above the behavioral testing area to allow the animal to move freely while receiving 450-nm blue light stimulations (Doric Lenses). To perform RTPT, mice were placed in a three-chamber rectangular apparatus (40.5 cm by 21 cm by 35 cm) with a central chamber and two side chambers (18 cm by 21 cm by 35 cm), each distinguished by different wall patterns (stripes versus dots). On a baseline day, mice explored the entire arena for 20 min without optical stimulation (off). Mice showing a side preference of more than 65% during the baseline test were excluded from further study. On a subsequent day, the mice were placed in the no-stimulation side of the arena, which was randomly assigned. The 20-min sessions began when the mouse fully crossed (all four paws) from the "no-stimulation" side to the "stimulation-paired side." Upon entering the stimulation-paired side, mice received blue light stimulation (20 Hz, 5-ms pulses) until returning to the no-stimulation side, at which point the stimulation ceased. The time spent in each chamber was assessed using a camera (Logitech) and video tracking software (Viewer 3.0, BIOBSERVE). The percentage of time spent in the stimulation-paired chamber was calculated as [(time in the stimulation-paired chamber) / (time in the stimulation-paired chamber + time in the no stimulation-paired chamber) × 100 (%)].

Circuit mapping quantification

Fluorescence-labeled fibers originating from vGlut2 RE or vCA1 neurons were quantified as previously described (*48*, *80*), with slight modifications. Coronal brain sections (50 μm) were collected along the AP axis of the brain, and brain regions were identified on the basis of anatomical landmarks and the Paxinos and Franklin mouse brain atlas (*81*). Imaging was taken using a Nikon SoRa spinning disk confocal microscope, and analysis was conducted in Fiji (ImageJ). The density of EGFP-expressing fibers was assessed as a percentage of the area of thresholded pixels normalized to injection sites of AAVretro-DIO-Flp (Fig. 5D) or AAVretro-Cre (Fig. 7, B and D). Threshold values were qualitatively determined by assessing the level that best mirrored the original image without introducing a background, and the same threshold was consistently applied to all images.

For RE inputs to either the vCA1➔BA or vCA1➔Hypoth neurons, coronal sections (50 μm) were collected along the AP axis of the brain and imaged using an Olympus VS120 slide scanner. mCherry-positive inputs were counted in the rostral RE (bregma, −0.58 to −0.82 mm), medial RE (bregma, −0.94 to −1.22 mm), and caudal RE (bregma, −1.34 to −1.58 mm). Data were presented as the percentage of mCherry-positive signals within each RE subdivision relative to the total mCherry-positive signals quantified across the entire rostral-to-caudal RE.

CTB-positive neurons were quantified using the "Cell Counter" function in Fiji (ImageJ). Data were calculated as the percentage of cell labeled with only CTB-488, only CTB-647, or both CTB-488 and CTB-647, relative to the total CTB-positive cells within each rostral, medial, and caudal RE, as described above.

Statistical analysis

Animals used in this study were not selected on the basis of prerequisite features other than general animal well-being (for example, regular grooming and locomotion and no apparent infections) for allocation into a particular experimental group. Differences across more than two groups were analyzed with one-way or two-way analysis of variance (ANOVA), followed by Bonferroni or Fisher's least significant difference post hoc tests for multiple comparisons. For comparisons between two groups, two-tailed unpaired *t* tests were used, as described in the figure legends. The distribution of data was checked for normality and equal variance. $P < 0.05$ was considered statistically significant. Data are reported as the means ± SEM. All statistical tests were performed using SigmaStat software (version 4.0, Inpixon). Detailed statistical information for datasets in Figs. 1 to 7 were summarized in table S1.

Supplementary Materials

The PDF file includes:
Figs. S1 to S11
Legend for movie S1
Legend for table S1

Other Supplementary Material for this manuscript includes the following:
Movie S1
Table S1

REFERENCES AND NOTES

1. T. C. Harford, H. Yi, B. F. Grant, Associations between childhood abuse and interpersonal aggression and suicide attempt among U.S. Adults in a national study. *Child Abuse Negl.* **38**, 1389–1398 (2014).
2. X. Fang, P. S. Corso, Child maltreatment, youth violence, and intimate partner violence. *Am. J. Prev. Med.* **33**, 281–290 (2007).
3. A. E. Russell, C. Joinson, E. Roberts, J. Heron, T. Ford, D. Gunnell, P. Moran, C. Relton, M. Suderman, B. Mars, Childhood adversity, pubertal timing and self-harm: A longitudinal cohort study. *Psychol. Med.* **52**, 3807 (2021).
4. M. Shafti, P. J. Taylor, A. Forrester, D. Pratt, The co-occurrence of self-harm and aggression: A cognitive-emotional model of dual-harm. *Front. Psychol.* **12**, 586135 (2021).
5. M. Shafti, S. Steeg, D. de Beurs, D. Pratt, A. Forrester, R. T. Webb, P. J. Taylor, The inter-connections between self-harm and aggressive behaviours: A general network analysis study of dual harm. *Front. Psych.* **13**, 953764 (2022).
6. O. O'Donnell, A. House, M. Waterman, The co-occurrence of aggression and self-harm: Systematic literature review. *J. Affect. Disord.* **175**, 325–350 (2015).
7. H. Sahlin, R. Kuja-Halkola, J. Bjureberg, P. Lichtenstein, Y. Molero, M. Rydell, E. Hedman, B. Runeson, J. Jokinen, B. Ljótsson, C. Hellner, Association between deliberate self-harm and violent criminality. *JAMA Psychiatry* **74**, 615–621 (2017).
8. A. Hetzenauer, M. J. Sinnegger-Brauns, J. Striessnig, N. Singewald, Brain activation pattern induced by stimulation of L-type Ca^{2+}-channels: Contribution of $Ca_V1.3$ and $Ca_V1.2$ isoforms. *Neuroscience* **139**, 1005–1015 (2006).
9. K. Klaus, K. Butler, H. Gutierrez, S. J. Durrant, K. Pennington, Interactive effects of early life stress and CACNA1C genotype on cortisol awakening response. *Biol. Psychol.* **136**, 22–28 (2018).
10. Z. D. Kabir, A. Martínez-Rivera, A. M. Rajadhyaksha, From gene to behavior: L-type calcium channel mechanisms underlying neuropsychiatric symptoms. *Neurotherapeutics* **14**, 588–613 (2017).
11. S. Heyes, W. S. Pratt, E. Rees, S. Dahimene, L. Ferron, M. J. Owen, A. C. Dolphin, Genetic disruption of voltage-gated calcium channels in psychiatric and neurological disorders. *Prog. Neurobiol.* **134**, 36–54 (2015).
12. P. L. Bader, M. Faizi, L. H. Kim, S. F. Owen, M. R. Tadross, R. W. Alfa, G. C. L. Bett, R. W. Tsien, R. L. Rasmusson, M. Shamloo, Mouse model of Timothy syndrome recapitulates triad of autistic traits. *Proc. Natl. Acad. Sci. U.S.A.* **108**, 15432–15437 (2011).
13. B. F. Kania, B. Dębski, D. Wrońska, E. Zawadzka, Verapamil - L type voltage gated calcium channel inhibitor diminishes aggressive behavior in male Siamese fighting fish. *Pol. J. Vet. Sci.* **18**, 401–406 (2015).
14. Z. D. Kabir, A. Che, D. K. Fischer, R. C. Rice, B. K. Rizzo, M. Byrne, M. J. Glass, N. V. De Marco Garcia, A. M. Rajadhyaksha, Rescue of impaired sociability and anxiety-like behavior in adult cacna1c-deficient mice by pharmacologically targeting eIF2α. *Mol. Psychiatry* **22**, 1096–1109 (2017).
15. J. F. Hayes, A. Lundin, S. Wicks, G. Lewis, I. C. K. Wong, D. P. J. Osborn, C. Dalman, Association of hydroxylmethyl glutaryl coenzyme a reductase inhibitors, L-type calcium channel antagonists, and biguanides with rates of psychiatric hospitalization and self-harm in individuals with serious mental illness. *JAMA Psychiatry* **76**, 382–390 (2019).
16. L. Colbourne, P. J. Harrison, Brain-penetrant calcium channel blockers are associated with a reduced incidence of neuropsychiatric disorders. *Mol. Psychiatry* **27**, 3904–3912 (2022).

17. H. A. Jinnah, S. Yitta, T. Drew, B. S. Kim, J. E. Visser, J. D. Rothstein, Calcium channel activation and self-biting in mice. *Proc. Natl. Acad. Sci. U.S.A.* **96**, 15228–15232 (1999).
18. S. Shoob, N. Buchbinder, O. Shinikamin, O. Gold, H. Baeloha, T. Langberg, D. Zarhin, I. Shapira, G. Braun, N. Habib, I. Slutsky, Deep brain stimulation of thalamic nucleus reuniens promotes neuronal and cognitive resilience in an Alzheimer's disease mouse model. *Nat. Commun.* **14**, 1–17 (2023).
19. S. S. Guo, Y. Gong, T. T. Zhang, X. Y. Su, Y. J. Wu, Y. X. Yan, Y. Cao, X. L. Song, J. C. Xie, D. Wu, Q. Jiang, Y. Li, X. Zhao, M. X. Zhu, T. Le Xu, M. G. Liu, A thalamic nucleus reuniens-lateral septum-lateral hypothalamus circuit for comorbid anxiety-like behaviors in chronic itch. *Sci. Adv.* **10**, 6272 (2024).
20. D. Li, H. Du, S. T. Qu, J. L. Wu, Y. C. Li, Q. Y. Xu, X. Chen, X. X. Dai, J. T. Xu, Q. Wang, G. Y. Xu, Thalamic nucleus reuniens glutamatergic neurons mediate colorectal visceral pain in mice via 5-HT2B receptors. *Neurosci. Bull.* **40**, 1421–1433 (2024).
21. Z. Chen, Y. Han, Z. Ma, X. Wang, S. Xu, Y. Tang, A. L. Vyssotski, B. Si, Y. Zhan, A prefrontal-thalamic circuit encodes social information for social recognition. *Nat. Commun.* **15**, 1036 (2024).
22. M. Bohic, L. A. Pattison, Z. A. Jhumka, H. Rossi, J. K. Thackray, M. Ricci, N. Mossazghi, W. Foster, S. Ogundare, C. R. Twomey, H. Hilton, J. Arnold, M. A. Tischfield, E. A. Yttri, E. St. John Smith, I. Abdus-Saboor, V. E. Abraira, Mapping the neuroethological signatures of pain, analgesia, and recovery in mice. *Neuron* **111**, 2811–2830.e8 (2023).
23. A. Upadhyay, M. A. Gradwell, T. J. Vajtay, J. Conner, A. A. Sanyal, C. Azadegan, K. R. Patel, J. K. Thackray, M. Bohic, F. Imai, S. O. Ogundare, Y. Yoshida, I. Abdus-Saboor, E. Azim, V. E. Abraira, The dorsal column nuclei scale mechanical sensitivity in naive and neuropathic pain states. *Cell Rep.* **44**, 115556 (2025).
24. I. Abdus-Saboor, N. T. Fried, M. Lay, J. Burdge, K. Swanson, R. Fischer, J. Jones, P. Dong, W. Cai, X. Guo, Y. X. Tao, J. Bethea, M. Ma, X. Dong, L. Ding, W. Luo, Development of a mouse pain scale using sub-second behavioral mapping and statistical modeling. *Cell Rep.* **28**, 1623–1634.e4 (2019).
25. J. M. Jones, W. Foster, C. R. Twomey, J. Burdge, O. M. Ahmed, T. D. Pereira, J. A. Wojick, G. Corder, J. B. Plotkin, I. Abdus-Saboor, A machine-vision approach for automated pain measurement at millisecond timescales. *eLife* **9**, e57258 (2020).
26. L. Berkowitz, Pain and aggression: Some findings and implications. *Motiv. Emot.* **17**, 277–293 (1993).
27. Y. Wang, L. Li, J. Cai, H. Li, C. Wang, Incidental physical pain reduces brain activities associated with affective social feedback and increases aggression. *Soc. Cogn. Affect. Neurosci.* **18**, nsac048 (2023).
28. P. Ziobro, Y. Woo, Z. He, K. Tschida, Midbrain neurons important for the production of mouse ultrasonic vocalizations are not required for distress calls. *Curr. Biol.* **34**, 1107–1113.e3 (2024).
29. J. Ruat, A. J. Genewsky, D. E. Heinz, S. F. Kaltwasser, N. S. Canteras, M. Czisch, A. Chen, C. T. Wotjak, Why do mice squeak? Toward a better understanding of defensive vocalization. *iScience* **25**, 104657 (2022).
30. E. S. McCoy, S. K. Park, R. P. Patel, D. F. Ryan, Z. J. Mullen, J. J. Nesbitt, J. E. Lopez, B. Taylor-Blake, K. A. Vanden, J. L. Krantz, W. Hu, R. L. Garris, M. G. Snyder, L. V. Lima, S. G. Sotocinal, J. S. Austin, A. D. Kashlan, S. Shah, A. K. Trocinski, S. S. Pudipeddi, R. M. Major, H. O. Bazick, M. R. Klein, J. S. Mogil, G. Wu, M. J. Zylka, Development of PainFace software to simplify, standardize, and scale up mouse grimace analyses. *Pain* **165**, 1793–1805 (2024).
31. D. J. Langford, A. L. Bailey, M. L. Chanda, S. E. Clarke, T. E. Drummond, S. Echols, S. Glick, J. Ingrao, T. Klassen-Ross, M. L. Lacroix-Fralish, L. Matsumiya, R. E. Sorge, S. G. Sotocinal, J. M. Tabaka, D. Wong, A. M. J. M. Van Den Maagdenberg, M. D. Ferrari, K. D. Craig, J. S. Mogil, Coding of facial expressions of pain in the laboratory mouse. *Nat. Methods* **7**, 447–449 (2010).
32. M. U. Werner, F. M. Perkins, K. Holte, J. L. Pedersen, H. Kehlet, Effects of gabapentin in acute inflammatory pain in humans. *Reg. Anesth. Pain Med.* **26**, 322–328 (2001).
33. W. M. O'Brien, G. F. Bagby, Carprofen: A new nonsteroidal antiinflammatory drug pharmacology, clinical efficacy and adverse effects. *Pharmacotherapy* **7**, 16–24 (1987).
34. H. L. M. Ruel, R. Watanabe, M. C. Evangelista, G. Beauchamp, J. P. Auger, M. Segura, P. V. Steagall, Pain burden, sensory profile and inflammatory cytokines of dogs with naturally-occurring neuropathic pain treated with gabapentin alone or with meloxicam. *PLOS ONE* **15**, e0237121 (2020).
35. F. van den Boogert, B. Sizoo, P. Spaan, S. Tolstra, Y. H. A. Bouman, W. J. G. Hoogendijk, S. J. Roza, Sensory processing and aggressive behavior in adults with autism spectrum disorder. *Brain Sci.* **11**, 95 (2021).
36. T. M. Cummins, O. English, H. Minnis, D. Stahl, R. C. O. Connor, K. Bannister, S. B. McMahon, D. Ougrin, Assessment of somatosensory function and self-harm in adolescents. *JAMA Netw. Open* **4**, e2116853 (2021).
37. P. Paribello, M. Manchia, F. Pinna, B. Carpiniello, Impulsivity, aggressivity and mood disorders: A narrative review. *J. Psychopathol.* **30**, 62–72 (2024).
38. C. X. Peh, S. Shahwan, R. Fauziana, M. V. Mahesh, R. Sambasivam, Y. J. Zhang, S. H. Ong, S. A. Chong, M. Subramaniam, Emotion dysregulation as a mechanism linking child maltreatment exposure and self-harm behaviors in adolescents. *Child Abuse Negl.* **67**, 383–390 (2017).
39. V. Kafetzopoulos, N. Kokras, I. Sotiropoulos, J. F. Oliveira, H. Leite-Almeida, A. Vasalou, V. M. Sardinha, Z. Papadopoulou-Daifoti, O. F. X. Almeida, K. Antoniou, N. Sousa, C. Dalla, The nucleus reuniens: A key node in the neurocircuitry of stress and depression. *Mol. Psychiatry* **23**, 579–586 (2018).
40. M. J. Dolleman-Van Der Weel, A. L. Griffin, H. T. Ito, M. L. Shapiro, M. P. Witter, R. P. Vertes, T. A. Allen, The nucleus reuniens of the thalamus sits at the nexus of a hippocampus and medial prefrontal cortex circuit enabling memory and behavior. *Learn. Mem.* **26**, 191–205 (2019).
41. J. T. McKenna, R. P. Vertes, Afferent projections to nucleus reuniens of the thalamus. *J. Comp. Neurol.* **480**, 115–142 (2004).
42. R. W. Reynolds, Equivalence of radio frequency and electrolytic lesions in producing septal rage. *Psychon. Sci.* **2**, 35–36 (1965).
43. L. C. Wong, L. Wang, J. A. D'Amour, T. Yumita, G. Chen, T. Yamaguchi, B. C. Chang, H. Bernstein, X. You, J. E. Feng, R. C. Froemke, D. Lin, Effective modulation of male aggression through lateral septum to medial hypothalamus projection. *Curr. Biol.* **26**, 593–604 (2016).
44. D. Lin, M. P. Boyle, P. Dollar, H. Lee, E. S. Lein, P. Perona, D. J. Anderson, Functional identification of an aggression locus in the mouse hypothalamus. *Nature* **470**, 221–226 (2011).
45. A. L. Falkner, P. Dollar, P. Perona, D. J. Anderson, D. Lin, Decoding ventromedial hypothalamic neural activity during male mouse aggression. *J. Neurosci.* **34**, 5971–5984 (2014).
46. J. L. Bubier, D. A. G. Drabick, Co-occurring anxiety and disruptive behavior disorders: The roles of anxious symptoms, reactive aggression, and shared risk processes. *Clin. Psychol. Rev.* **29**, 658–669 (2009).
47. I. D. Neumann, A. H. Veenema, D. I. Beiderbeck, Aggression and anxiety: Social context and neurobiological links. *Front. Behav. Neurosci.* **4**, 928 (2010).
48. S. Shin, I. J. You, M. Jeong, Y. Bae, X. Y. Wang, M. L. Cawley, A. Han, B. K. Lim, Early adversity promotes binge-like eating habits by remodeling a leptin-responsive lateral hypothalamus–brainstem pathway. *Nat. Neurosci.* **26**, 79–91 (2022).
49. D. D. Francis, J. Diorio, P. M. Plotsky, M. J. Meaney, Environmental enrichment reverses the effects of maternal separation on stress reactivity. *J. Neurosci.* **22**, 7840–7843 (2002).
50. M. Lippmann, A. Bress, C. B. Nemeroff, P. M. Plotsky, L. M. Monteggia, Long-term behavioural and molecular alterations associated with maternal separation in rats. *Eur. J. Neurosci.* **25**, 3091–3098 (2007).
51. A. R. Nectow, M. V. Moya, M. I. Ekstrand, A. Mousa, K. L. McGuire, C. E. Sferrazza, B. C. Field, G. S. Rabinowitz, K. Sawicka, Y. Liang, J. M. Friedman, N. Heintz, E. F. Schmidt, Rapid molecular profiling of defined cell types using viral TRAP. *Cell Rep.* **19**, 655–667 (2017).
52. D. G. Ehlinger, K. G. Commons, Cav1.2 L-type calcium channels regulate stress coping behavior via serotonin neurons. *Neuropharmacology* **144**, 282–290 (2018).
53. Y. Zhang, E. Garcia, A. S. Sack, T. P. Snutch, L-type calcium channel contributions to intrinsic excitability and synaptic activity during basolateral amygdala postnatal development. *J. Neurophysiol.* **123**, 1216–1235 (2020).
54. E. J. Nunes, N. A. Addy, L-type calcium channel regulation of dopamine activity in the ventral tegmental area to nucleus accumbens pathway: Implications for substance use, mood disorders and co-morbidities. *Neuropharmacology* **224**, 109336 (2023).
55. T. P. Snutch, J. Peloquin, E. Mathews, J. E. McRory, *Molecular Properties of Voltage-Gated Calcium Channels* (Landes Bioscience, 2013).
56. R. P. Vertes, W. B. Hoover, A. C. Do Valle, A. Sherman, J. J. Rodriguez, Efferent projections of reuniens and rhomboid nuclei of the thalamus in the rat. *J. Comp. Neurol.* **499**, 768–796 (2006).
57. T. D. Viena, G. E. Rasch, D. Silva, T. A. Allen, Calretinin and calbindin architecture of the midline thalamus associated with prefrontal-hippocampal circuitry. *Hippocampus* **31**, 770–789 (2021).
58. C. Varela, S. Kumar, J. Y. Yang, M. A. Wilson, Anatomical substrates for direct interactions between hippocampus, medial prefrontal cortex, and the thalamic nucleus reuniens. *Brain Struct. Funct.* **219**, 911–929 (2014).
59. W. B. Hoover, R. P. Vertes, Collateral projections from nucleus reuniens of thalamus to hippocampus and medial prefrontal cortex in the rat: A single and double retrograde fluorescent labeling study. *Brain Struct. Funct.* **217**, 191–209 (2012).
60. J. C. Jimenez, K. Su, A. R. Goldberg, V. M. Luna, J. S. Biane, G. Ordek, P. Zhou, S. K. Ong, M. A. Wright, L. Zweifel, L. Paninski, R. Hen, M. A. Kheirbek, Anxiety cells in a hippocampal-hypothalamic circuit. *Neuron* **97**, 670–683.e6 (2018).
61. J. C. Jimenez, J. E. Berry, S. C. Lim, S. K. Ong, M. A. Kheirbek, R. Hen, Contextual fear memory retrieval by correlated ensembles of ventral CA1 neurons. *Nat. Commun.* **11**, 3492 (2020).
62. M. M. Gergues, K. J. Han, H. S. Choi, B. Brown, K. J. Clausing, V. S. Turner, I. D. Vainchtein, A. V. Molofsky, M. A. Kheirbek, Circuit and molecular architecture of a ventral hippocampal network. *Nat. Neurosci.* **23**, 1444–1452 (2020).

63. F. Bai, L. Huang, J. Deng, Z. Long, X. Hao, P. Chen, G. Wu, H. Wen, Q. Deng, X. Bao, J. Huang, M. Yang, D. Li, Y. Ren, M. Zhang, Y. Xiong, H. Li, Prelimbic area to lateral hypothalamus circuit drives social aggression. *iScience* **26**, 107718 (2023).
64. L. A. Schwarz, K. Miyamichi, X. J. Gao, K. T. Beier, B. Weissbourd, K. E. Deloach, J. Ren, S. Ibanes, R. C. Malenka, E. J. Kremer, L. Luo, Viral-genetic tracing of the input–output organization of a central noradrenaline circuit. *Nature* **524**, 88–92 (2015).
65. G. Corder, B. Ahanonu, B. F. Grewe, D. Wang, M. J. Schnitzer, G. Scherrer, An amygdalar neural ensemble that encodes the unpleasantness of pain. *Science* **363**, 276–281 (2019).
66. L. J. Becker, C. Fillinger, R. Waegaert, S. H. Journée, P. Hener, B. Ayazgok, M. Humo, M. Karatas, M. Thouaye, M. Gaikwad, L. Degiorgis, M. des Neiges Santin, M. Mondino, M. Barrot, E. C. Ibrahim, G. Turecki, R. Belzeaux, P. Veinante, L. A. Harsan, S. Hugel, P. E. Lutz, I. Yalcin, The basolateral amygdala-anterior cingulate pathway contributes to depression-like behaviors and comorbidity with chronic pain behaviors in male mice. *Nat. Commun.* **14**, 2198 (2023).
67. T. Camps, M. Amat, V. M. Mariotti, S. Le Brech, X. Manteca, Pain-related aggression in dogs: 12 clinical cases. *J. Vet. Behav.* **7**, 99–102 (2012).
68. R. A. Sansone, J. D. Sinclair, M. W. Wiederman, Self-harm behavior among chronic pain patients. *Prim. Care Companion J. Clin. Psychiatry* **11**, 362 (2009).
69. J. A. Prior, Z. Paskins, R. Whittle, A. Abdul-Sultan, C. A. Chew-Graham, S. Muller, R. Bajpai, T. A. Shepherd, A. Sumathipala, C. D. Mallen, Rheumatic conditions as risk factors for self-harm: A retrospective cohort study. *Arthritis Care Res.* **73**, 130–137 (2021).
70. B. Kuriya, S. Vigod, J. Luo, J. Widdifield, N. Haroon, The risk of deliberate self-harm following a diagnosis of rheumatoid arthritis or ankylosing spondylitis: A population-based cohort study. *PLOS ONE* **15**, e0229273 (2020).
71. E. A. Selby, A. Kranzler, J. Lindqvist, K. B. Fehling, J. Brillante, F. Yuan, X. Gao, A. L. Miller, The dynamics of pain during nonsuicidal self-injury. *Clin. Psychol. Sci.* **7**, 302–320 (2019).
72. M. C. Nowycky, A. P. Fox, R. W. Tsien, Long-opening mode of gating of neuronal calcium channels and its promotion by the dihydropyridine calcium agonist Bay K 8644. *Proc. Natl. Acad. Sci. U.S.A.* **82**, 2178–2182 (1985).
73. N. Scheel, P. Wulff, J. G. de Mooij-van Malsen, Afferent connections of the thalamic nucleus reuniens in the mouse. *J. Comp. Neurol.* **528**, 1189–1202 (2020).
74. H. J. van Oers, E. R. de Kloet, S. Levine, Early vs. late maternal deprivation differentially alters the endocrine and hypothalamic responses to stress. *Brain Res. Dev. Brain Res.* **111**, 245–252 (1998).
75. S. A. Golden, M. Heshmati, M. Flanigan, D. J. Christoffel, K. Guise, M. L. Pfau, H. Aleyasin, C. Menard, H. Zhang, G. E. Hodes, D. Bregman, L. Khibnik, J. Tai, N. Rebusi, B. Krawitz, D. Chaudhury, J. J. Walsh, M. H. Han, M. L. Shapiro, S. J. Russo, Basal forebrain projections to the lateral habenula modulate aggression reward. *Nature* **534**, 688–692 (2016).
76. W. Hong, D. W. Kim, D. J. Anderson, Antagonistic control of social versus repetitive self-grooming behaviors by separable amygdala neuronal subsets. *Cell* **158**, 1348–1361 (2014).
77. Y. Guo, X. Tang, J. Zhang, S. Jin, J. Li, L. Ding, K. Zhang, C. Yang, H. Zhou, X. He, F. Xu, G. Q. Bi, L. Xu, P. M. Lau, Corticosterone signaling and a lateral habenula–ventral tegmental area circuit modulate compulsive self-injurious behavior in a rat model. *J. Neurosci.* **38**, 5251–5266 (2018).
78. J. Jung, J. Ohk, H. Kim, C. E. Holt, H. J. Park, H. Jung, mRNA transport, translation, and decay in adult mammalian central nervous system axons. *Neuron* **111**, 650–668.e4 (2023).
79. C. Li, C. Miao, Y. Ge, J. Wu, P. Gao, S. Yin, P. Zhang, H. Yang, B. Tian, W. Chen, X. Q. Chen, A molecularly distinct cell type in the midbrain regulates intermale aggression behaviors in mice. *Theranostics* **15**, 707–725 (2025).
80. D. Knowland, V. Lilascharoen, C. P. Pacia, S. Shin, E. H. J. Wang, B. K. Lim, Distinct ventral pallidal neural populations mediate separate symptoms of depression. *Cell* **170**, 284–297. e18 (2017).
81. G. Paxinos, K. B. J. Franklin, *The Mouse Brain in Stereotaxic Coordinates* (Academic Press, ed. 3, 2008).
82. S. Shin, H. Pribiag, V. Lilascharoen, D. Knowland, X. Y. Wang, B. K. Lim, Drd3 signaling in the lateral septum mediates early life stress-induced social dysfunction. *Neuron* **97**, 195–208. e6 (2018).
83. I. J. You, Y. Bae, A. R. Beck, S. Shin, Lateral hypothalamic proenkephalin neurons drive threat-induced overeating associated with a negative emotional state. *Nat. Commun.* **14**, 6875 (2023).

Acknowledgments: We thank J. Colon for assisting with SLEAP pose estimation and computational analysis. We thank M. Ahrens for helping in vivo calcium imaging data analysis. We thank S. Fraser, S. McClafferty, C. Harrop, and A. Han for analyzing behavioral data. We thank M. Milam for technical assistance with molecular experiments and brain histology. We thank E. Mccoy and M. Zilka for guidance and scientific input in using PainFace software. **Funding:** This work was supported in part by grants from National Institutes of Health (NIH) grants R01DK132566 and R01MH137465-01A1 to S.S., Fralin Biomedical Research Institute Seale Innovation to S.S., the integrated translational Health Research Institute of Virginia (iTHRIV) funding in part by the National Center for Advancing Translational Sciences, NIH, through grant KL2TR003016/UL1TR003015 to S.S., and National Research Foundation of Korea (NRF) grant RS-2023–00214418 to J.J. **Author contributions:** Conceptualization: J.J., I.-J.Y., and S.S. Methodology: J.J., I.-J.Y., and S.S. Investigation: J.J., I.-J.Y., and S.S. Visualization: J.J. and S.S. Supervision: S.S. Writing—original draft: J.J., I.-J.Y., and S.S. Writing—review and editing: J.J. and S.S. **Competing interests:** The authors declare that they have no competing interests. **Data and materials availability:** All data needed to evaluate the conclusions in the paper are present in the paper and/or the Supplementary Materials. Custom MATLAB scripts supporting the findings of this study and dataset have been deposited in the Zenodo: 10.5281/zenodo.16790563.

Submitted 26 April 2025
Accepted 3 October 2025
Published 5 November 2025
10.1126/sciadv.ady5540

ScienceAdvances

Thalamo-hippocampal pathway determines aggression and self-harm

Jane Jung, In-Jee You, and Sora Shin

Sci. Adv. **11** (45), eady5540. DOI: 10.1126/sciadv.ady5540

Science Advances (ISSN 2375-2548) is published by the American Association for the Advancement of Science. 1200 New York Avenue NW, Washington, DC 20005. The title *Science Advances* is a registered trademark of AAAS.